resources

MDPI

Article

Evaluating Coal Quality and Trace Elements of the Karagandy Coal Formation (Kazakhstan): Implications for Resource Utilization and Industry

Medet Junussov [1,*], Geroy Zh. Zholtayev [2,*], Ahmed H. Moghazi [3], Yerzhan Nurmakanov [4], Mohamed Abdelnaby Oraby [5], Zamzagul T. Umarbekova [2], Moldir A. Mashrapova [2] and Kuanysh Togizov [2]

1 School of Mining and Geosciences, Nazarbayev University, Astana 010000, Kazakhstan
2 Institute of Geological Sciences Named after K.I. Satpayev, Almaty 050000, Kazakhstan
3 Institute of Earth Sciences, University of Iceland, 101 Reykjavík, Iceland
4 Core Facilities, Nazarbayev University, Astana 010000, Kazakhstan
5 Department of Geology, Faculty of Science, Ain Shams University, Cairo 11566, Egypt
* Correspondence: medet.junussov@nu.edu.kz (M.J.); zholtaev.geroy@mail.ru (G.Z.Z.)

Abstract

The Carboniferous coal seams in Northeast Kazakhstan remain insufficiently investigated, with a lack of comprehensive mineralogical and geochemical assessments necessary to understand the geological processes controlling coal quality. This study examines 15 coal samples from the Karagandy Coal Formation (KCF) at the Saradyr and Bogatyr mines using proximate and ultimate analyses, FTIR, XRD, SEM–EDS, ED-XRF, and ICP-OES, providing the first detailed comparison of mineralogical and geochemical characteristics—including depositional signals and inorganic constituent distribution—between these mines within the KCF. The coals exhibit an average ash yield of 24.1% on a dry basis, volatile matter of 21.6% on a dry and ash-free basis, and low moisture content of 1.1% (air-dry), with low sulfur levels of 0.7% in whole coal across both mines. Mineralogical composition is dominated by quartz and clay minerals, with minor pyrite, apatite, chalcopyrite, and rutile. Major oxides in the coal ash average 68.2% SiO_2 and 19.5% Al_2O_3, followed by Fe_2O_3, K_2O, and TiO_2 (3–12.1%). Among the 24 identified trace elements, Sm is the most abundant at 6.3 ppm with slight enrichment (CC = 2.8), Lu remains at normal levels (CC < 1), and most other elements are depleted (CC < 0.5). The Al_2O_3/TiO_2 ratios (3.8–10.8) indicate contributions from intermediate to mafic parent materials. The detrital mineralogy, parting compositions, and elevated ash content indicate significant accommodation space development during or shortly after peat accumulation, likely within a vegetated alluvial plain depression. These findings provide new insights into the depositional environment and coal-forming processes of the KCF and contribute to regional assessments of coal quality and resource potential.

Keywords: coal mineralogy; Kazakhstan; Carboniferous coal; trace elements; REE

Check for updates

Academic Editor: Benjamin McLellan

Received: 27 November 2025
Revised: 19 December 2025
Accepted: 23 December 2025
Published: 25 December 2025

Copyright: © 2025 by the authors. Licensee MDPI, Basel, Switzerland. This article is an open access article distributed under the terms and conditions of the Creative Commons Attribution (CC BY) license.

1. Introduction

The detailed mineralogical and elemental characterization of coal is essential for its effective utilization, environmental management, quality assessment, development of processing methodologies, and resource exploration [1–3]. Coal is a complex blend of organic and inorganic constituents formed from the transformation of organic matter, characterized by a diverse composition of minerals and chemical elements [4–9]. Major

inorganic elements (e.g., Al, Si, Ti, Fe, Ca) are typically present at concentrations above 0.1 wt%, while trace elements (e.g., As, V, Cu, Zn, Pb, REEs, U) generally occur below 0.1 wt%, ranging from 1 ppb to several hundred ppm [2–4]. Inorganic constituents in coal originate from three primary sources: dissolved salts in water-filled pores of low-rank coals, elements bound to organic compounds forming chelates, and mineral compounds [4,10–12]. Understanding the distribution of these inorganic components provides valuable geological insights into coal deposition and holds economic significance for the exploration of essential trace elements, including rare earth and radioactive metals [13–15]. This knowledge also informs practical applications, including mining, processing, combustion, and utilization, helping to mitigate technological challenges such as abrasion, corrosion, fouling, and slagging, and supports the assessment of environmental and health impacts as well as industrial uses in cement production, wastewater treatment, and element recovery [12–15].

Kazakhstan, the 10th largest coal producer globally, comprises nine coal basins with estimated total reserves of approximately 150 Gt, of which 28.2 Gt are recoverable [16–19]. The largest and economically viable reserves are typically Carboniferous in age. Recent studies report elevated levels of valuable metals in coal deposits across Central and Northeastern Kazakhstan. The Shubarkol coal deposit shows high concentrations of rare earth elements such as Y (254 ppm), Nd (806 ppm), La (46 ppm), and Gd (335 ppm), whereas earlier investigations in the Karagandy coal basin reported lower values (Y up to 54 ppm, Sc up to 43 ppm, U at 6.4 ppm, Th at 11.4 ppm) [20–22]. Coal from the Ekibastuz basin also contains elevated Ti and Zr (up to 1%), Y (up to 30 ppm), U (2.5 ppm), and Th (3.1 ppm) [16–18].

The Karagandy Coal Formation (KCF) is among the most important coal formations in Kazakhstan, occurring in the largest Carboniferous basins of Karagandy, Teniz-Korzhynkol, and Ekibastuz [16–18]. Coal from KCF is a key energy source for power generation, heating, and steel production. While mineralogical and geochemical studies have been conducted on coals from the Karagandy basin [20,22–25], similar research is limited for the Teniz-Korzhynkol and Ekibastuz basins. The KCF includes multiple workable seams in two active mines: Saradyr (Teniz-Korzhynkol) and Bogatyr (Ekibastuz), producing bituminous coals with high ash yield (25.7–50% dry basis) and medium volatile matter (22–35% dry and ash free basis) [16,18,25]. Petrographic studies indicate a predominance of vitrinite with minor inertinite, and vitrinite reflectance (Ro%) values range from 0.5 to 1.3%, corresponding to sub-bituminous to high-volatile bituminous ranks [16,18,25].

Despite these investigations on general coal quality, detailed studies on the mineralogical and geochemical characteristics of KCF coals remain limited, particularly regarding inorganic constituents and their implications for depositional conditions and coal-forming processes. Addressing this gap is essential for a comprehensive understanding of KCF coals and their potential industrial applications.

This study provides a detailed assessment of inorganic components in coals from Saradyr and Bogatyr mines, examining their mineralogical and elemental composition, modes of occurrence, resource potential, and environmental implications. The high ash yields in these seams likely result from geological factors such as detrital input during peat accumulation, fluvial–deltaic flooding, volcanic ash incorporation, and diagenetic groundwater activity, which facilitated the formation of authigenic minerals. By filling this knowledge gap, the study aims to enhance understanding of Kazakh coal resources and support future industrial utilization and environmentally responsible management.

2. Geological Settings

The study area is specifically associated with the Early Carboniferous KCF. Both mines are located within the KCF, which are part of the larger coal basins: Teniz-Korzhynkol for the Saradyr mine and Ekibastuz for the Bogatyr mine (Figures 1 and 2a,b).

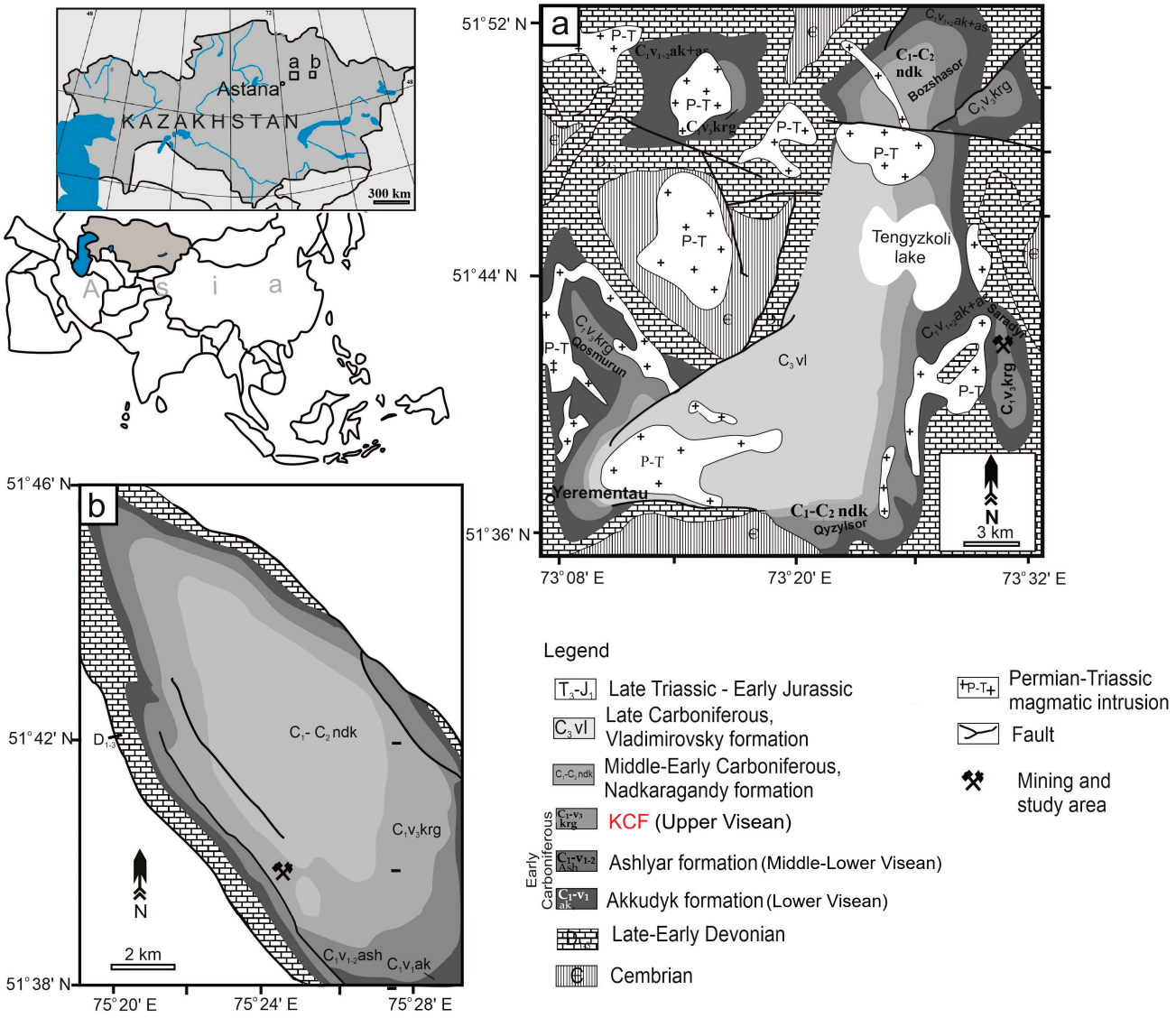


Figure 1. Geological maps showing (**a**) Teniz-Korzhynkol coal basin with the Saradyr coal mine, and (**b**) Ekibastuz coal basin with the Bogatyr coal mine (modified after [16]), both located within the Karagandy Coal Formation (KCF; highlighted in red).

The geological evaluation of the Carboniferous coal basins of Teniz-Korzhynkol and Ekibastuz has been extensively documented by numerous authors [16,18,25]. The basins preserve distinct sedimentary sequences, characterized by marine carbonate-clay sediments at their lowest horizons, formed during the Devonian period, which serve as the basement rocks for the overlying Carboniferous formations, transitioning upwards to a thick complex of continental sandy-clayey coal-bearing sediments. During the Carboniferous period, a climatic transition occurred, marked by a shift from a humid environment in the Lower Carboniferous to a warmer and drier climate in the Upper Carboniferous that resulted in a change in coal deposits [26]. Notably, North-East Kazakhstan saw significant coal accumulation due to structural conditions in intermountain depressions and troughs, particularly in the largest coal basins of Kazakhstan, such as Teniz-Korzhynkol and Ek-

ibastuz [16]. The Early-Middle Carboniferous formations were the most productive across these basins [23,24,26].

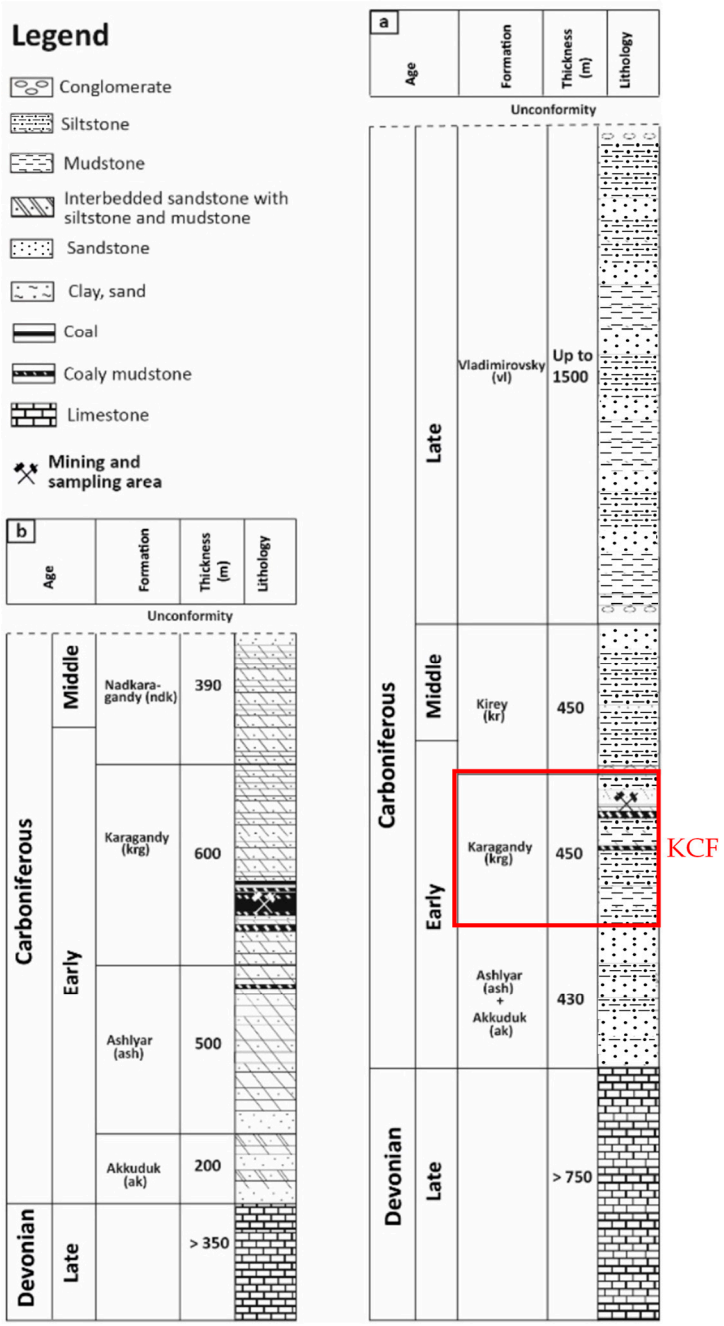


Figure 2. Stratigraphic sequences of two basins within the studied mines at the KCF (shown within the red framework): (**a**) Teniz-Korzhynkol coal basin showing the Saradyr coal mine, and (**b**) Ekibastuz coal basin showing the Bogatyr coal mine (modified after [16]), with sampling area indicated.

The Teniz-Korzhynkol coal basin occurs as a large brachysynclinal structure (20 × 20 km) with a total estimated coal reserve of about 2.6 Gt, including four small syncline structures of Qosmurun, Qyzylsor, Bozshasor, and Saradyr, formed as coal deposits, currently extracted exclusively through open-cast mining at the Saradyr coal deposit (extending over 8 km^2) (Figure 1a). The coal basin hosts about 60–70 coal seams. The coal seam thickness fluctuates from 1.5 to 3.0 m. The depth of coal occurrences in the basin reaches up to 1800 m below the surface. The basin is characterized by a significant presence of Permian-Triassic magmatic intrusions, mainly as dikes and sills, primarily consisting of granite-porphyry

compositions. Within the Devonian basement, major sedimentary formations include limestone, shale, and marl, typically with a thickness of 200 m. Coal seams are found within the Upper Carboniferous Vladimirovsky formation and followed by the Early Carboniferous formations of Karagandy, Ashlyar, and Akkuduk, occurring alongside sedimentary rocks like clay, marl, mudstone, sandstone, and siltstone.

The Ekibastuz coal basin is characterized by an asymmetrical graben-syncline (8.5 × 24 km), extending from the northwest to the southeast, it is bounded by major faults oriented in the same direction within the basin. A total estimated coal reserve of about 9.7 Gt. The basin contains around 6 workable coal seams and 15 unworkable coal seams. In this study, only Seam 1 from the Bogatyr mine was considered. The thickness of coal seams in the basin ranges from 8 to 30 m. The maximum depth of coal occurrences ranges between 530 m and 680 m below the surface. Early Carboniferous sequences in this basin comprise coal-bearing formations such as Nadkaraganda, Karagandy, Ashlyar, and Akkuduk, interbedded with dark gray mudstone, siltstone, and green fine-grained sandstones.

Both Early Carboniferous basins filling start with the Akkuduk Formation (C_1 ak), which is non-productive, while productive coal formations extend from the Ashlyar to the Karagandy Coal Formations across both basins. The Karagandy Coal Formation (KCS) remains notably productive, with currently accessible and exploitable coal seams [16,18,25].

3. Samples and Methods

3.1. Sample Selection

Sampling was conducted across two operational coal mines Saradyr and Bogatyr situated in northeast Kazakhstan. A total of fifteen samples were collected, each obtained exclusively from minable seams within these mines, covering two coal seams within the Karagandy Coal Formation (KCF). The distance between the two mines is approximately 260 km. Both coal seams exhibit relatively simple structural settings with gentle bedding and no major fault disturbances. The sampled seams show a thickness variation of approximately 1.5–3.0 m, allowing reliable vertical profiling. Based on previous regional studies, the coals fall within the low- to medium-rank metamorphism category, typical for the KCF. Correlation between the Saradyr and Bogatyr seams is supported by their consistent lithological characteristics, shared formation age, and similar stratigraphic positioning within the KCF.

Five samples from the Saradyr open-cast coal mine (near Yerementau town, Akmola region) were collected from a single main coal seam at depths ranging from 250 to 260 m, and ten samples from the Bogatyr coal mine (near Ekibastuz city, Pavlodar region) were collected from a single main seam at depths of approximately 140–160 m (Figure 3a,b). The samples were collected using the grab sampling method, with vertical intervals of 0.2–0.5 m within each seam to cover multiple stratigraphic sublayers (roof, middle, and floor sections), ensuring vertical representativeness.

To capture the full variability of each seam, sampling was performed across the entire seam thickness, targeting different stratigraphic horizons. Samples were collected from areas far from lithological rock layers to avoid contamination and to ensure the collection of pure coal. In addition, locations were selected to reflect typical coal quality and lithology within each seam. This comprehensive sampling approach ensures that the collected samples provide a representative and reliable overview of coal properties across both mines.

All samples were stored in plastic bags to minimize potential contamination and oxidation. Coal samples were labeled according to their mine of origin and their stratigraphic position within the coal seam. Samples from the Saradyr mine are labeled as S (from Saradyr) and numbered from S1 to S5, representing different stratigraphic horizons, whereas samples from the Bogatyr mine are labeled as B (from Bogatyr) and numbered

from B1/0 to B1/9, representing successive horizons. This labeling scheme reflects both the sampling location and the relative vertical position within the coal seam, from top to bottom. This stratigraphic labeling also facilitates correlation and comparison between the sampled seams from the two mines, further supporting the representativeness and purity of the dataset.

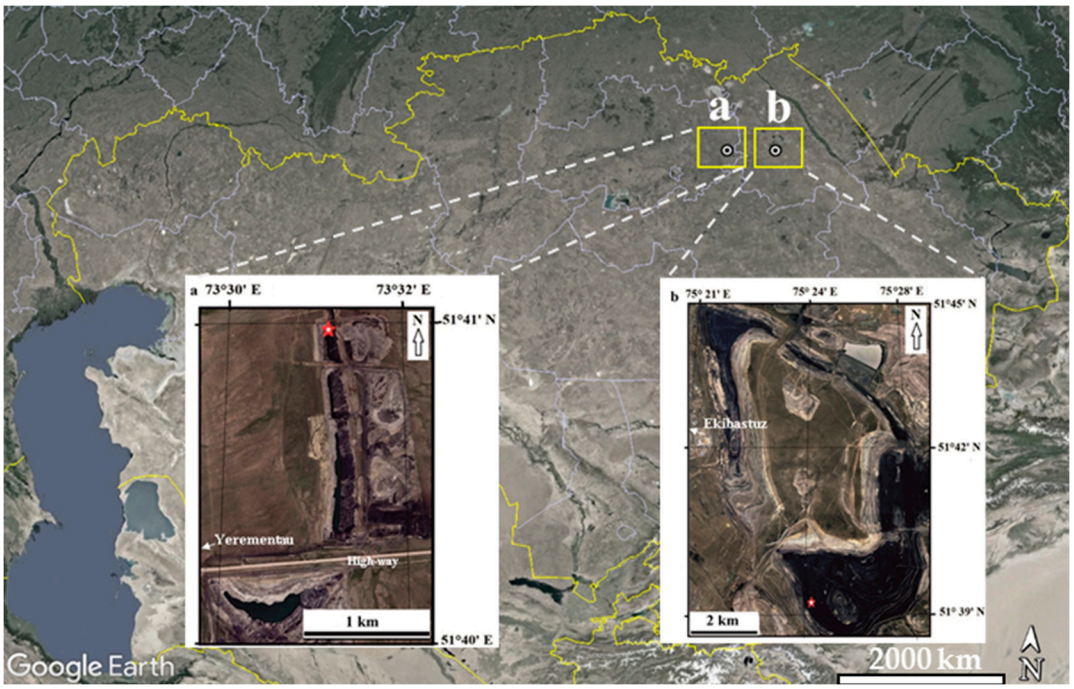


Figure 3. Overview map of two active coal mines: (**a**) Saradyr and (**b**) Bogatyr. The star symbols indicate the locations of two mines (a satellite map, Google Earth Pro 7.3).

3.2. Sample Preparation

All coal samples from the two mines were prepared as polished blocks, finely powdered coal, and coal ash. Fifteen polished epoxy-bound particulate pellets were prepared according to standard procedures [27] to identify minerals in coal samples using electron microscopy(JEOL, Shojima, Tokyo, Japan).

The powdered coal samples were prepared for geochemical analysis using the standard coal sample preparation procedures as follows in [28]. The powdered coal samples were prepared for a series of analyses, including proximate and ultimate analysis; mineral and functional groups analysis; and coal LTA (low-temperature ash) and HTA (high-temperature ash) samples for mineralogical and elemental composition.

For coal ash samples: 2 g of each sample were accurately weighed and crushed to particle sizes between approximately 50 to 200 μm using an agate mortar and pestle, to exclude any contaminations. Two types of coal ash samples: the LTA, 150 °C for 18 h [29] and the HTA (initially at 500 °C for 30 min, followed by heating at 815 °C for 1 h) were prepared in a muffle furnace(Carbolite ELF 11, Carbolite Gero, Neuhausen, Germany), based on [30].

3.3. Analytical Procedure

Proximate analysis, covering moisture, volatile matter, and ash yield, was performed according to American Society for Testing and Materials (ASTM) Standards [31–33]. For the determination of ultimate analysis, intervals of selected elements including C, H, N, and S were analyzed following [34], utilizing an organic elemental analyzer (OEA, Elementar UNICUBE, Frankfurt, Germany). The gross calorific value of coal was estimated using proximate and

ultimate analyses, based on the methods of [35,36]. The determination of total sulfur and its forms was conducted in accordance with ASTM Standards [37,38], respectively.

Fourier transform infrared analysis (FTIR): the identification of minerals in coals were examined using a Nicolet iS10 FTIR spectrometer (Thermo Nicolet Corp., Madison, WI, USA), equipped with a diamond/ZnSe crystal plate. Spectra were acquired in the mid-infrared range in absorbance mode, covering wavelengths from 4500 to 450 cm^{-1}.

Scanning electron microscopy with energy dispersive spectroscopy (SEM-EDS): fifteen polished blocks were investigated under a SEM-EDS (Jeol JSM-IT200 LA, JEOL, Shojima, Tokyo, Japan) to observe mineral characteristics and to determine elemental distribution in the coal samples. The operating parameters were set to 20 kV acceleration voltage and high vacuum mode.

X-ray diffractometer (XRD): minerals in the coal were determined using low-temperature ashes (LTA) of coal on a Rigaku SmartLab XRD machine(Rigaku, Akishima-shi, Tokyo, Japan) with a Ni-filtered Cu Kα X-ray source (energy 8.04 keV and x-ray wavelength 1.5406 Å) and XRD pattern was recorded with a step size of 0.01°, over a 2θ interval of 2.6–70° [39]. The XRD evaluation of the LTA was conducted at room temperature. The X-ray diffractograms of all coal samples were subjected for quantitative mineralogical analysis using the Rietveld Refinement method, based on the [40,41], and the utilized XRD database for phase identification within COD (Crystallography Open Database) and AMCSD (American Mineralogist Crystal Structure Database).

Energy dispersive X-ray fluorescence (ED-XRF) was employed to measure major element using an Epsilon 4 spectrometer (Malvern PANalytical, Malvern, UK, max 50 kV/2 mA/10 W). Converted to oxides High-temperature (815 °C) coal ash samples were used for this analysis. The procedures followed [42], and the equipment's reliability has been discussed by [43].

Inductively coupled plasma optical emission spectroscopy (ICP-OES, Thermo Fisher Scientific iCAP RQ, Waltham, Massachusetts, USA) equipment to determine the quantities of trace elements. Fifteen coal samples, each weighing 0.1 g, underwent the 5 mL HNO_3 and 1 mL of H_2O_2, proposed in reference [44]. The heating of samples was up to 180 °C for 1 h in a hot block digestion system (HotBlock 200), and made syringe filtration with a 0.45-micron filter (Sterile Millex-HV Millipore, Merck Millipore, Darmstadt, Germany). The filtrated liquids were then analyzed using ICP-OES. The digestion of International Reference Materials and blanks involved preparation and analysis following the same procedure.

All analyses were conducted at the Core Facilities and laboratories of the School of Mining and Geosciences, Nazarbayev University in Astana, Kazakhstan, except for LTA-XRD identification and quantification, which were performed at the Faculty of Science, Ain Shams University, Cairo, Egypt.

4. Results

4.1. Proximate and Ultimate Analyses

The proximate analysis results for the 15 coal samples from two coal mines exhibit slight differences from each other, with the overall moisture contents ranging between 0.2% and 4.1% (average 1.1%), and volatile matter ranging between 16% and 29.7% (average 21.6%), while ash yield ranging from 10.7 to 40.6% with an average of 24.1%. The total sulfur content in coal samples range from 0.48 to 1.17% (average 0.68%), suggesting that these coals generally exhibit lower sulfur content relative to coals reported from other regions worldwide. Organic sulfur forms were more prevalent (average 0.37%) than sulfide sulfur (average 0.21%), followed by sulfate sulfur (average 0.1%) in coal samples from both mines. In terms of ultimate analysis, the samples are primarily composed of carbon (C), followed by hydrogen (H), with nitrogen (N) present in smaller proportions. The content

range for elemental composition is as follows: C ranges from 47.2 to 73.8% (average 57.3%), H from 2.0 to 4.7% (average 3.6%), and N from 0.5 to 1.8% (1.0%), indicating that it is of bituminous rank (Table 1).

Table 1. Results of proximate and ultimate analyses, sulfur forms (unit, wt%), calorific values (unit, MJ/kg) for coal samples.

Samples	M (Ad)	V (daf)	A (db)	Q_{gr} (Ad)	C (daf)	H (daf)	N (daf)	S_t (db)	S_p (db)	S_s (db)	S_o (db)
S1	0.5	24.7	19.3	19.5	56.3	3.3	0.7	0.58	0.01	0.06	0.5
S2	1.1	22.1	40.6	19.7	50.0	3.0	0.6	0.65	0.3	0.05	0.3
S3	4.1	28.6	18.7	17.4	54.3	3.1	0.5	1.15	0.79	0.06	0.3
S4	1.3	20.0	39.1	21.0	52.3	3.3	0.7	0.63	0.13	bdl	0.5
S5	1.2	23.7	17.0	15.8	50.0	3.3	0.7	1.07	0.31	0.26	0.5
B1/0	0.2	16.0	16.5	14.9	51.6	2.0	0.7	0.83	0.09	0.24	0.5
B1/1	1.1	29.7	25.2	30.4	70.7	4.7	1.8	0.71	0.15	0.16	0.4
B1/2	1.2	21.0	24.9	24.2	62.1	3.7	1.3	0.5	0.27	0.03	0.2
B1/3	1.3	19.3	29.7	22.5	57.9	3.4	1.2	0.65	0.19	0.06	0.4
B1/4	0.4	17.1	10.7	13.0	47.2	3.1	0.9	0.51	0.21	bdl	0.3
B1/5	1.2	23.7	11.2	28.6	73.8	4.3	1.5	0.65	0.05	0.2	0.4
B1/6	1.2	20.1	28.5	25.0	55.9	6.3	1.0	0.53	0.15	0.18	0.2
B1/7	1.1	23.1	24.3	24.1	61.6	3.9	1.3	0.48	0.17	0.01	0.3
B1/8	1.1	23.1	16.6	24.5	68.6	4.1	1.3	0.66	0.2	0.06	0.4
B1/9	0.4	22.8	40.6	19.2	48.5	3.0	0.9	0.6	0.19	0.01	0.4
Average	1.1	21.6	24.1	21.3	57.3	3.6	1.0	0.68	0.21	0.10	0.37

Note: M—moisture; V—volatile matter; A—ash yield; Q_{gr}—gross calorific value; C—carbon; H—hydrogen; N—nitrogen; S_t—total sulfur; S_p—sulfide sulfur; S_s—sulfate sulfur; S_o—organic sulfur; Ad-air-dry basis; db—dry basis; daf—dry and ash—free basis; bdl—below detection limit.

4.2. Distribution of Functional Groups

Using FTIR (Figure 4), the results of coal molecular structures and their chemical bonds indicate that the main functional groups present in the selected coal samples (S1 and B1/0) include hydroxyl, aromatic, aliphatic, and oxygen-containing functional groups. These particular samples were selected because they are representative of the Saradyr and Bogatyr coal seams, covering the range of coal ranks and mineralogical characteristics in the study area, and thus provide insight into the variability of molecular structures within the KCF. The functional groups were identified based on their absorption peaks in the FTIR spectra. Specifically, the hydroxyl and aliphatic absorption peak is observed at 2919 cm^{-1}, while the absorption peak corresponding to the aromatic structures (methyl groups (CH3) and carboxyl groups (C=O)) is found in the range of 1437 to 1598 cm^{-1}. The slight increase in aromaticity observed in the FTIR spectra of the samples suggests that the coal has undergone a significant degree of coalification, leading to the enrichment of aromatic compounds. Quartz and clay minerals exhibit characteristic absorption bands between 777 and 1005 cm^{-1} in the samples, based on [45–47]. FTIR analysis has effectively characterized mineral matter in coals [47,48], while XRD has identified mineral phases in coal samples [47].

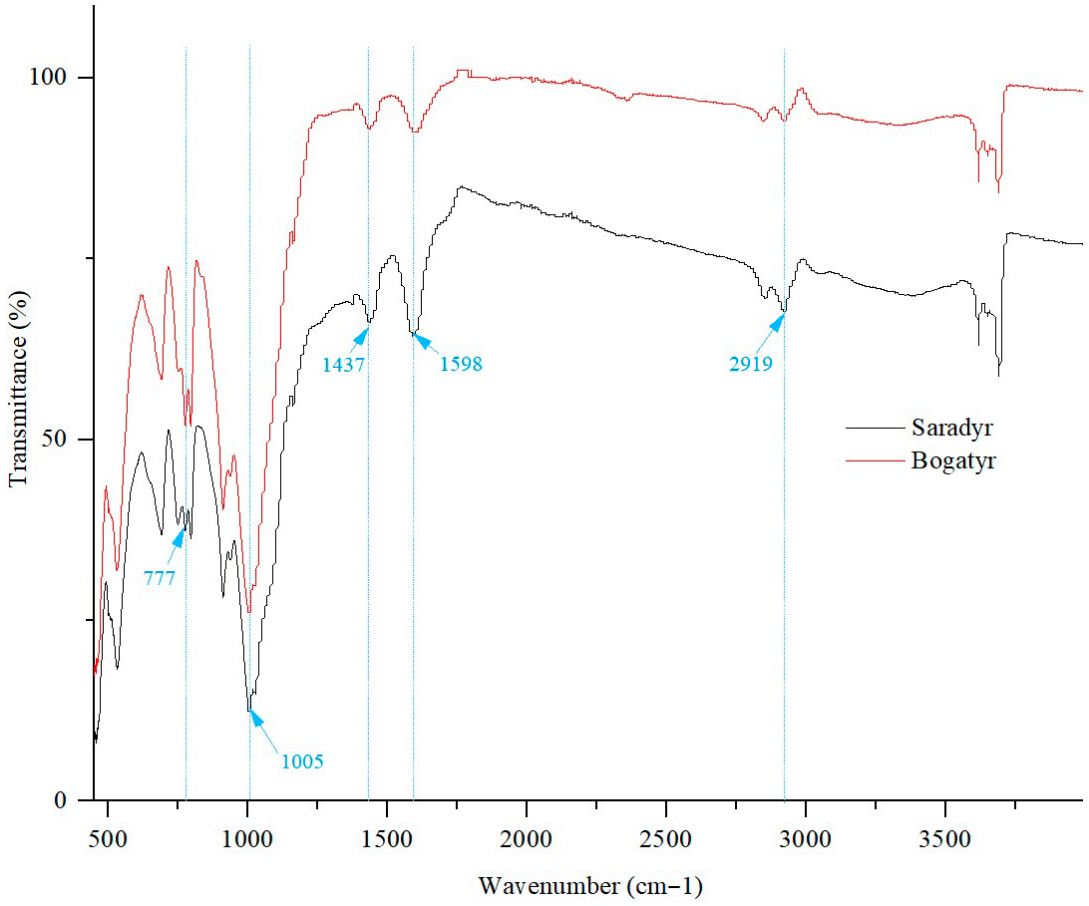


Figure 4. FTIR spectra of the selected coal samples (S1 and B1/0) from the Saradyr and Bogatyr coal mines.

4.3. Mineralogical Analysis of Coal: LTA-XRD and SEM-EDS

The mineral percentages in the LTAs of the coal samples are detailed in Table 2 and Figure 5. The LTA mineral matter from both mines predominantly comprises quartz, averaging 85.2 wt%. Clay minerals are of significant importance, with average compositions including 11.8 wt% kaolinite, 1.0 wt% smectite, and 5.0 wt% illite. Siderite is found in the LTA samples from both mines, with an average of 6.7 wt%, while halite is a minor component in the Saradyr samples, averaging 2.9 wt%. Only four representative samples are shown in Figure 5 because they correspond to the top and bottom horizons of the coal seams and capture the main vertical mineralogical variability. The remaining samples exhibit either very similar XRD patterns and mineral phases occurring in very minor amounts that are not readily distinguishable in the diffraction patterns.

SEM-EDS results show (see Figure 6a,i) that the samples from Saradyr and Bogatyr primarily consist of quartz grains with a size of around 25 µm, along with kaolinite distributed along the bedding planes and in the cleats of coals. Illite minerals are predominantly associated with kaolinite, displaying a compact structure, while smectite exhibits irregular edges and a rough surface, often found in association with barite crystals in the samples from both mines. Barite in the samples precipitates within fractures and nanopores of the coal, often forming elongated crystals with slightly rough surfaces, and is associated with clay minerals. Additionally, halite occurs in association with clay minerals, forming thin films with small corroded areas, suggesting secondary alteration processes within the samples.

Table 2. Mineralogical compositions of all coal samples from the two coal mines measured by Low-temperature ashing X-ray diffraction (LTA-XRD, unit wt%).

Samples	Quartz	Kaolinite	Smectite	Illite	Siderite	Halite
S1	97	n.a.	n.a.	3.0	n.a.	n.a.
S2	88.8	n.a.	n.a.	11.2	n.a.	n.a.
S3	66.1	25.2	n.a.	n.a.	4.1	4.6
S4	86.0	10.0	0.4	n.a.	n.a.	n.a.
S5	70.0	14.7	n.a.	n.a.	14	1.3
B1/0	94.8	n.a.	n.a.	5.2	n.a.	n.a.
B1/1	99.2	n.a.	n.a.	0.8	n.a.	n.a.
B1/2	90.0	8.6	1.4	n.a.	n.a.	n.a.
B1/3	88.2	10.6	1.2	n.a.	n.a.	n.a.
B1/4	88.0	10.5	1.5	n.a.	n.a.	n.a.
B1/5	84.0	16.0	n.a.	n.a.	n.a.	n.a.
B1/6	69.6	28.7	1.7	n.a.	n.a.	n.a.
B1/7	80.0	18	n.a.	n.a.	2.0	n.a.
B1/8	86.0	13.5	0.5	n.a.	n.a.	n.a.
B1/9	91.0	8.5	0.5	n.a.	n.a.	n.a.
Average	84.4	11.8	1.0	5.0	6.7	2.9

Note: n.a.—data not available.

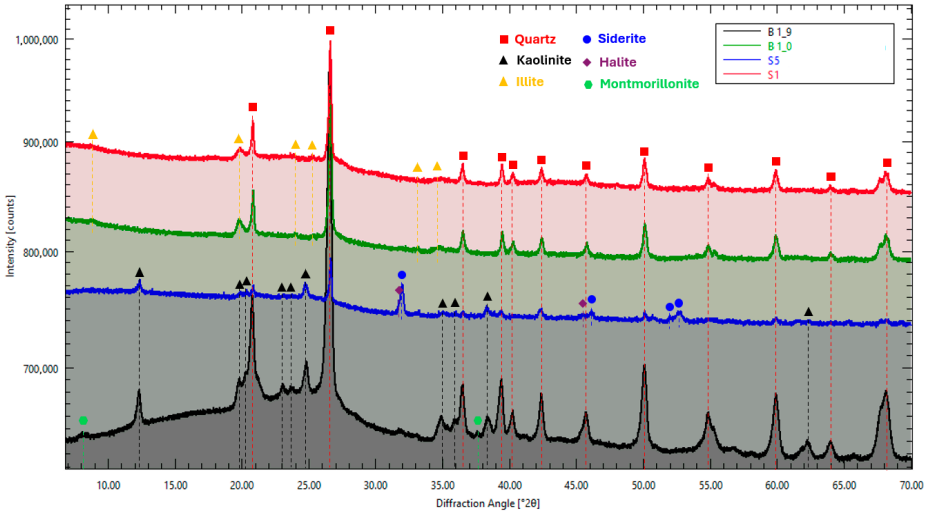


Figure 5. XRD patterns of LTA samples collected from the top and bottom of the coal seams in two coal mines. Identified mineral phases are marked in color: red—quartz; black—kaolinite; yellow—illite; blue—siderite; violet—halite; green—montmorillonite.

SEM-EDS shows accessory minerals (Figure 6b,f), including chalcopyrite, rutile, ilmenite, and REE (Ce)-bearing phosphate minerals in all samples of both mines. The accessory minerals are regularly found in association with kaolinite crystal grains, were identified through SEM-EDS analysis as cleat/pore-infilling minerals within the coal matrix.

Additionally, minor amounts of euhedral pyrite, with sizes of up to 10 μm, are observed in the samples. Accessory minerals, including apatite (2–4 μm), Ce-bearing phosphate crystal (5 μm), barite and chalcopyrite (up to 10 μm) were observed within the kaolinite grains. Additionally, a small proportion of titanium dioxide mineral (3 μm)

and ilmenite (2 µm) were identified as detrital minerals within the deformed cells of coal materials in both mine samples.

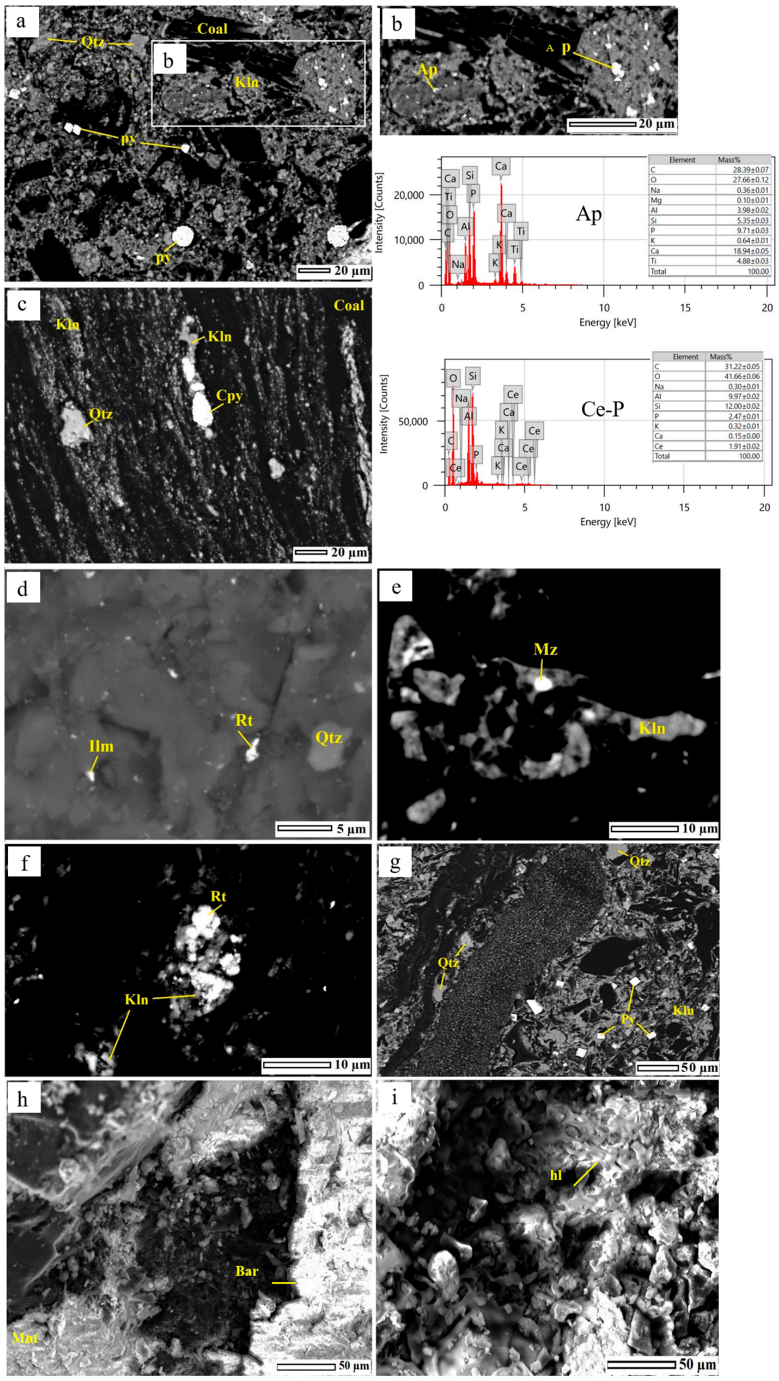


Figure 6. Selected SEM-BSE images of crystalline phases and EDS spectra of coal samples: (**a**) crystal growth of apatite (Ap) crystals among framboidal and euhedral pyrites (py) associated with kaolinite (kln) matrix, and (**b**) individual apatite crystals with the EDS spectrum and elemental concentrations, from B1/0; (**c**) chalcopyrite (Cpy) grains with kaolinite, surrounded by illite (ill) and quartz (Qtz) minerals, from B1/1; (**d**) individual crystals of ilmenite (Ilm) and rutile (Rt), as well as quartz growth occurring within coal fractures, and (**e**) crystal grains of Ce-bearing phosphate mineral (Ce-P) associated with kaolinite matrix with the EDS spectrum and elemental concentrations, from S1; (**f**) individual crystals of rutile with kaolinite, and (**g**) euhedral pyrites associated with kaolinite matrix, from S2; (**h**) barite (Bar) crystals with surrounding smectite (Mnt), and (**i**) crystal grains of halite (hl), from S4.

The apatite and Ce-bearing phosphate crystals were characterized by their association with kaolinite, as well as the association of kaolinite with organic matter within the samples. The apatite and Ce-bearing phosphate minerals, such as detrital minerals, are intermixed with the kaolinite. The apatite crystals have a comparatively smaller size (up to 4 μm) than other Ce-bearing phosphate crystals (5 μm) in the samples of both coal deposits.

4.4. Major and Trace Element Analysis of Coal

Table 3, and Figures 7 and 8 present the concentrations of major and trace elements in the coal samples from two coal mines, analyzed using ED-XRF and ICP-OES.

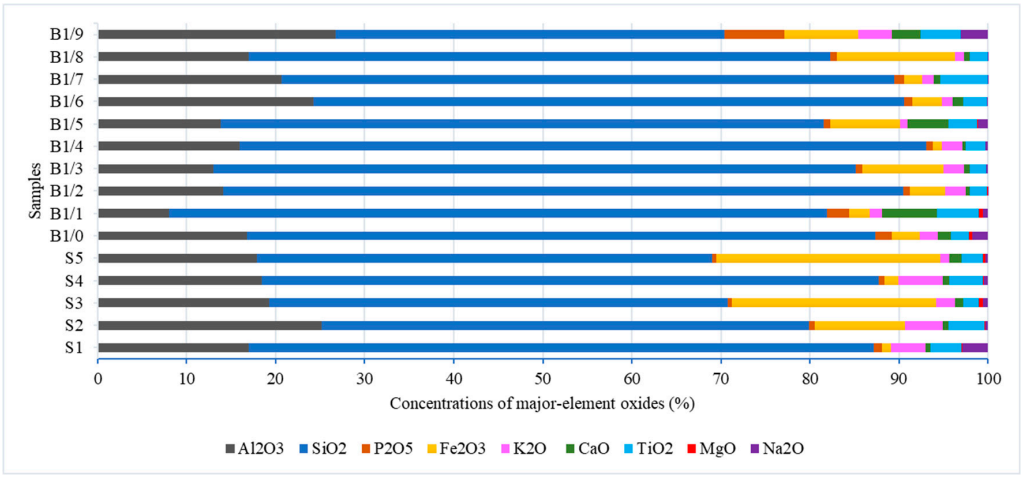


Figure 7. Major-element oxide composition of coal samples from the Saradyr (S1–S5) and Bogatyr (B1/0–B1/9) mines.

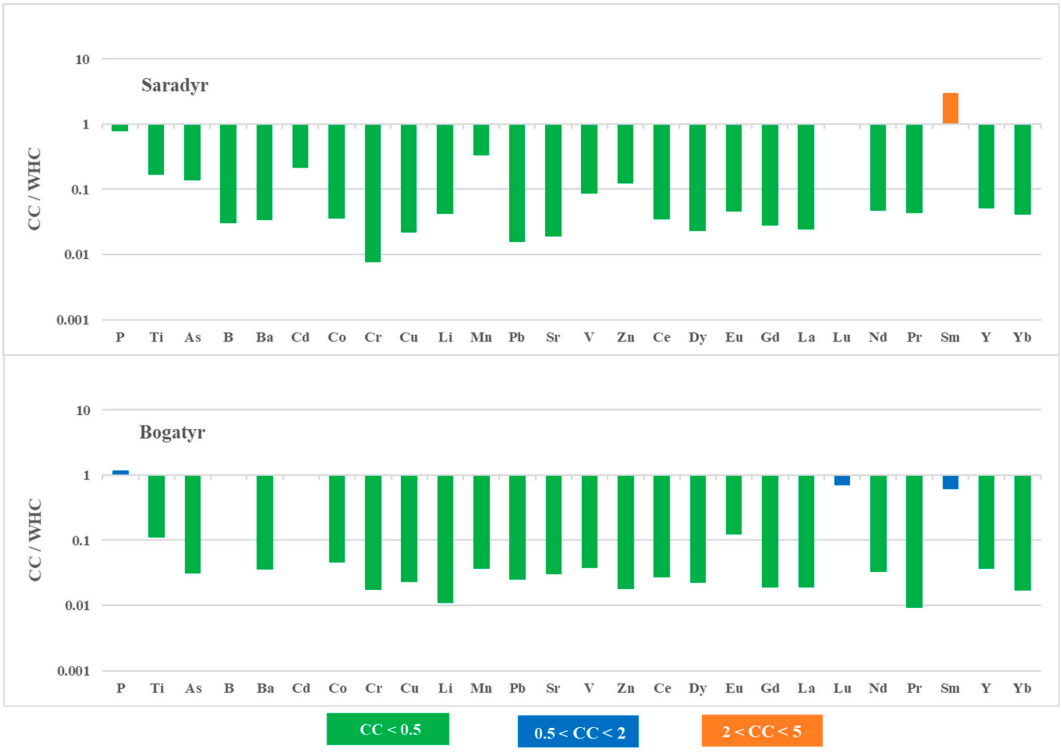


Figure 8. Concentration coefficients (CC) of major elements (P and Ti) and trace elements in coals from both Saradyr and Bogatyr mines, normalized by the average concentrations of major/trace elements in world hard coal (WHC [7]).

Table 3. ED-XRF analysis of coal ash samples for major elements (unit, % after conversion to oxides); and ICP-OES shows trace element concentrations (unit, ppm) of coal samples (*WHC values is based on [7], shown the average of major elements from world coal ash, and trace elements from world coal).

Elements	Saradyr Samples							Average	*WHC
	Wavelength, nm	LOQ, ppb	S1	S2	S3	S4	S5		
Al_2O_3%			16.9	25.1	19.2	18.4	17.8	19.5	nd
SiO_2%			70.2	54.7	51.4	69.2	51.1	59.3	nd
P_2O_5%			0.8	0.6	0.4	0.6	0.4	0.6	0.15
Fe_2O_3%			1.0	10.1	23	1.5	25	12.1	nd
Na_2O %			2.9	0.2	0.6	0.4	0.3	0.3	nd
K_2O %			3.8	4.1	2.1	4.9	1.0	3.2	nd
CaO %			0.5	0.6	0.8	0.7	1.3	0.8	nd
TiO_2%			3.4	3.9	1.7	3.8	2.3	3.0	5.3
MgO%			0.1	0.1	0.3	0.1	0.3	0.2	nd
As	396.15	4	bdl	bdl	bdl	1.27	bdl	1.2	9
B	249.67	10	2.52	bdl	1.09	2.0	0.18	1.4	47
Ba	455.40	0.05	8.41	0.52	0.5	16	0.57	5.2	150
Cd	214.43	0.2	bdl	0.04	0.03	bdl	0.06	0.04	0.2
Co	228.61	0.5	0.12	0.11	0.24	0.53	0.09	0.21	6
Cr	267.71	1	0.1	0.06	0.05	0.4	0.05	0.1	17
Cu	324.75	0.8	0.62	0.26	0.25	bdl	0.29	0.3	16
Li	670.78	3	1.46	bdl	0.36	0.31	0.26	0.5	14
Mn	257.61	0.1	3.6	36.5	26.2	0.6	52.4	23.8	71
Pb	220.35	3	0.11	0.19	0.02	0.11	0.29	1.9	9
Sr	421.55	0.04	0.63	0.84	0.61	2.1	5.46	1.9	100
V	292.40	5	2.07	1.46	1.06	5.0	2.7	2.4	28
Zn	206.20	0.3	11.27	0.44	5.51	0.38	0.32	3.5	28

Table 3. *Cont.*

Elements	Saradyr Samples							Average	*WHC
	Wavelength, nm	LOQ, ppb	S1	S2	S3	S4	S5		
Ce	456.23	5	0.62	0.4	0.78	1.9	0.39	0.8	23
Dy	353.17	0.5	0.03	bdl	bdl	0.07	bdl	0.05	2.1
Eu	381.96	2	0.01	bdl	bdl	0.03	bdl	0.02	0.4
Gd	335.04	2	0.06	0.06	0.08	0.14	0.05	0.07	2.7
La	412.32	7	0.07	bdl	0.24	0.5	0.0	0.2	11
Lu	291.13	5	bdl	bdl	bdl	bdl	bdl	bdl	0.2
Nd	406.10	20	bdl	0.26	0.69	1.37	0.01	0.5	12
Pr	414.31	3	0.1	bdl	bdl	0.2	bdl	0.1	3.4
Sm	330.63	6	1.52	9.08	6.24	2.55	12.5	6.3	2.2
Y	360.07	0.2	0.29	0.4	0.61	0.36	0.47	0.4	8.2
Yb	328.93	0.8	0.01	0.04	0.05	0.03	0.08	0.04	1
REY			18.2	23.6	39.2	14.4	29.6	25.3	67.2 **
SiO_2/Al_2O_3			4.1	2.1	2.6	3.7	2.8		

Elements	Bogatyr samples										Average	*WHC
	B1/0	B1/1	B1/2	B1/3	B1/4	B1/5	B1/6	B1/7	B1/8	B1/9		
Al_2O_3%	16.7	8.0	14.0	12.9	16.0	13.8	24.2	20.6	16.9	26.7	17.0	nd
SiO_2%	70.6	73.9	76.3	72.1	77.0	67.7	66.2	68.8	65.3	43.6	68.2	nd
P_2O_5%	1.8	2.4	0.7	0.7	0.7	0.7	0.9	1.0	0.7	6.6	1.6	0.15
Fe_2O_3%	3.1	2.3	3.9	9.0	1.0	7.8	3.3	2.0	13.3	8.3	5.4	nd
Na_2O	1.7	0.5	0.07	0.2	0.3	1.1	0.1	0.03	0.06	3.0	0.7	nd
K_2O %	2.0	1.4	2.3	2.2	2.2	0.8	1.2	1.2	1.0	3.7	1.8	nd
CaO %	1.4	4.4	0.5	0.6	0.3	4.4	1.1	0.7	0.5	3.1	1.8	nd

Table 3. *Cont.*

Elements	Bogatyr samples										Average	*WHC
	B1/0	B1/1	B1/2	B1/3	B1/4	B1/5	B1/6	B1/7	B1/8	B1/9		
TiO_2%	2.0	4.6	1.9	1.8	2.2	3.2	2.6	5.3	2.0	4.5	3.0	5.3
MgO%	0.4	0.4	0.03	bdl	bdl	0.06	bdl	bdl	bdl	bdl	0.09	nd
As	0.55	bdl	0.03	bdl	bdl	bdl	bdl	bdl	bdl	bdl	0.2	9
B	bdl	bdl	bdl	bdl	bdl	bdl	bdl	bdl	bdl	bdl	bdl	47
Ba	30	1.9	4.3	2.4	3.1	2.2	4.2	3.5	2.5	1.1	5.5	150
Cd	bdl	bdl	bdl	bdl	bdl	bdl	bdl	bdl	bdl	bdl	bdl	0.2
Co	0.39	0.12	0.26	0.13	0.06	0.08	1.34	0.18	0.17	0.11	0.1	6
Cr	0.21	bdl	0.19	bdl	bdl	bdl	bdl	0.14	0.94	0.05	0.3	17
Cu	1.32	0.12	0.26	0.13	0.06	0.08	1.32	0.18	0.17	0.11	0.3	16
Li	0.41	0.2	bdl	0.04	0.1	bdl	0.15	0.04	bdl	bdl	0.1	14
Mn	0.65	0.43	1.52	5.06	0.69	0.96	3.27	0.73	6.69	7.04	2.7	71
Pb	0.41	0.7	0.22	0.16	0.23	0.16	0.16	0.1	0.05	0.13	0.2	9
Sr	13.2	1.29	2.04	1.8	1.69	1.47	4.17	2.74	1.81	1.03	3.1	100
V	1.92	0.47	1.77	0.58	0.9	0.64	0.68	1.97	1.25	0.68	1.0	28
Zn	2.39	0.12	0.45	0.66	0.31	0.3	0.2	0.16	0.32	0.24	0.5	28
Ce	1.09	0.03	0.57	0.55	0.68	0.28	0.89	0.68	1.09	0.55	0.6	23
Dy	0.13	0.01	0.06	0.02	0.03	0.04	0.01	0.04	0.13	0.01	0.04	2.1
Eu	0.01	bdl	bdl	bdl	bdl	bdl	bdl	bdl	0.1	bdl	0.05	0.4
Gd	0.1	bdl	0.03	bdl	bdl	bdl	0.01	0.02	0.1	bdl	0.05	2.7
La	0.34	bdl	0.12	bdl	bdl	bdl	0.04	0.24	0.34	bdl	0.2	11
Lu	bdl	bdl	bdl	0.03	bdl	0.43	0.08	bdl	bdl	0.04	0.1	0.2
Nd	0.48	0.23	bdl	0.14	0.03	0.44	0.46	0.55	0.48	0.82	0.4	12
Pr	0.05	0.01	0.04	bdl	bdl	bdl	bdl	0.01	0.05	bdl	0.03	3.4

Table 3. *Cont.*

Elements	Bogatyr samples										Average	*WHC
	B1/0	B1/1	B1/2	B1/3	B1/4	B1/5	B1/6	B1/7	B1/8	B1/9		
Sm	2.2	0.55	1.59	1.93	0.65	1.36	0.71	0.92	2.2	1.81	1.3	2.2
Y	0.61	0.04	0.43	0.26	0.34	0.25	0.16	0.21	0.61	0.19	0.3	8.2
Yb	bdl	bdl	0.01	0.02	0.03	0.01	bdl	bdl	bdl	bdl	0.01	1
REY	21.4	23.1	17.7	18.2	8.4	16.8	7.5	16.4	21.5	12.4	16.7	67.2 **
SiO_2/Al_2O_3	4.2	9.2	5.4	5.5	4.8	4.9	2.7	3.3	3.8	1.6		

Note: LOQ—limit of quantification; bdl—below detection limit; nd-no data; ** Values calculated for a comparison of the same REY elements in the samples, based on WHC [7].

The examined samples of two mines reveal varying concentrations of major elements, with their respective ranges as shown in Table 3 and Figure 7. The samples from both coal mines predominantly contain high concentrations of major elements, with SiO_2 (68.2%) and Al_2O_3 (19.5%) showing high average values. In contrast, other major elements have lower concentrations within these samples, including Fe_2O_3 (12.1%), K_2O (3.2%), TiO_2 (3.0%), CaO (1.8%), P_2O_5 (1.6%), Na_2O (0.7%), and MgO (0.2%).

The most prevalent major element oxides in the samples are SiO_2 and Al_2O_3, with SiO_2 to Al_2O_3 ratio varying between 1.6 and 9.2 (Table 3). This suggests a significant presence of quartz and clay minerals.

In samples from both the Bogatyr and Saradyr mines, a total of 24 trace elements were analyzed, with manganese (Mn) being the most abundant, showing a maximum of 52.4 ppm in some Saradyr samples, while the average across all samples is 23.8 ppm. This is followed by Sm (6.3 ppm), Ba (5.5 ppm), Zn (3.5 ppm), Sr (3.1 ppm), V (2.4 ppm), Pb (1.9 ppm), B (1.4 ppm), As (1.2 ppm), Ce (0.8 ppm), Li and Nd (0.5 ppm), and Cu (0.3 ppm). It should be noted that Ba, while reaching up to 16 ppm in some samples, has an average of 5.2 ppm, slightly lower than the Mn average, with values generally higher in Saradyr than in Bogatyr. Other trace elements, typically present at averaged concentrations below 0.2 ppm, include Co, Cr, and Cd, following rare earth elements and yttrium (REY) with a decreasing concentration range from La, Lu, Dy, Eu, Gd, Pr, Y to Yb. REY concentrations in samples from both mines range from 7.5 to 39.2 ppm, with an average of 25.3 ppm, specifically related to the Saradyr samples.

Comparisons between the concentration averages of trace elements and the averages of world hard coal (WHC) [7] (Table 4 and Figure 8) reveal that Sm (average 6.3 ppm) in coal samples from both mines, exhibit higher averages than WHC for these elements, while the averages of remaining twenty-three elements in the samples are lower than those of WHC (shown in Figure 6). The averages for major elements are presented in Table 3, there is no further comparison with WHC as these elements are absent, except for P and Ti, which ranges in averages between 0.17% and 0.9% (no values in oxide form) in the coal ash samples from both mines. These averages are almost similar to or slightly higher than the P (0.15%) but lesser than Ti (5.3) of WHC. The *p* value may suggest that it is likely attributed to the presence of phosphate rare earth element minerals, as indicated by SEM-EDS analysis.

Table 4. Ratio Al_2O_3/TiO_2 for coal samples from both mines.

Ratio	Samples														
	S1	**S2**	**S3**	**S4**	**S5**	**B1/0**	**B1/1**	**B1/2**	**B1/3**	**B1/4**	**B1/5**	**B1/6**	**B1/7**	**B1/8**	**B1/9**
Al_2O_3/TiO_2	4.8	6.3	10.8	4.8	7.5	8.3	1.7	7.3	6.9	7.2	4.2	9	3.8	8.3	5.9

According to the method proposed by [49] for assessing the relative enrichment of trace elements, concentrations of trace elements in coal can be categorized into six groups: highly enriched (CC $\geq$ 100, where CC represents the concentration coefficient, indicating the ratio of trace-element concentrations in the samples being studied compared to the averages for WHC, significantly enriched (10 $\leq$ CC < 100), enriched (5 $\leq$ CC < 10), slightly enriched (2 $\leq$ CC < 5), normal (0.5 $\leq$ CC < 2), and depleted (CC < 0.5).

The Concentration Coefficient (CC) or enrichment factor of trace elements in our samples was determined by referencing the values established for World Hard Coal (WHC) by [7]. This enrichment factor helps ascertain whether elements are enriched or depleted by comparing the concentration of trace elements in our coal ash samples to the corresponding WHC values (Figure 8). While we aimed to calculate CCs for all major elements, most lacked corresponding WHC values for normalization. Consequently, we specifically measured the CCs for the major elements P and Ti. The element P has a CC between 0.5 and 1, placing it

in the normal concentration category, while Ti has a CC below 0.5, indicating it falls into the depleted category.

Trace elements in both mine samples, including Sm (with CC 2.8) falls into the slightly enriched category in the samples of Saradyr, but in the Bogatyr samples, Sm and Lu have CCs higher than 0.5; while the other twenty-two trace elements have CCs lower than 0.5, indicating their classification into the depleted category in samples from both mines.

5. Discussion

5.1. Depositional Environment

Coal undergoes natural weathering at low temperatures, leading to alteration in both its organic and inorganic components [50,51]. Most samples from both coal mines exhibit weathering conditions, although those from both mines show some signs of siderite, framboidal pyrite, and halite film forms in only a few coal samples. The siderite minerals in coals are found in association with elements such as Mn, Mg, and Ca (Figure 9a,b). As [52] noted, the presence of siderite in coals alongside elements like Mn, Mg, Ca, and Ba indicates fluid movements and chemical changes during coal formation. Another intriguing observation is the presence of pyrite framboids exclusively in Bogatyr samples, contrasting with their absence in Saradyr samples (Figure 7). The presence of framboidal pyrite, as suggested by studies [53,54], indicates favorable conditions for rapid sulfurization and iron sulfide mineral precipitation during peat accumulation. Rapid burial of organic-rich sediments, may create environments conducive to framboidal pyrite formation by limiting oxygen exposure and preserving organic matter. Additionally, the retention of cellular or microstructural features by framboidal pyrites, as noted in research [55,56], suggests their formation within the peat environment before coalification. This association with organic matter further supports their origin during or shortly after peat accumulation in the studied coal samples (Figure 9c).

The film forms of halite with small corroded portions was found in the Saradyr samples; however, this presence was not detectable using the XRD technique from the Bogatyr samples due to its low concentration. Only, the SEM-EDS analysis detected a low presence of halite with thin film forms in the sample B1/4 (Figure 9d). Findings of halite in thin films in some samples in both mines, can be attributed to secondary alteration processes involving the percolation of saline fluids through coal seams, as mentioned by [57]. These saline fluids can deposit halite as thin films on the surfaces of coal particles or within pores and fractures.

Although chemical analysis indicates low sulfate sulfur contents ranging from 0.01% (B1/9) to 0.79% (S3), with an average of 0.01%, corresponding sulfate minerals are not detected in the XRD patterns, except for siderite. This discrepancy is attributed to the fact that these minor sulfur amounts may occur as finely dispersed or amorphous phases, which are below the detection limits of XRD and other analytical techniques.

The depositional characteristics of minerals in coals of the Karagandy Formation, as revealed by LTA-XRD and SEM-EDS analyses indicate that quartz is a predominant mineral in coal samples obtained from both mines. According to [58], quartz grains typically indicate a detrital origin, suggesting that they were transported and deposited into the coal-forming environment. This suggests that the minerals found in the coal underwent alteration processes after being weathered and eroded from their original parent material before being deposited. The combination of detrital quartz grains and framboidal pyrite in the coals explains about how the environment changed over time. The detrital quartz likely came from through rivers or streams [59], which need a lot of energy. On the other hand, framboidal pyrite forms in quieter, low-energy settings [55]. This suggests that the detrital quartz was brought in during the early peat forming stage and the framboidal pyrite

formed during the early maturation process under reducing conditions. These findings show how the coal formed and the changes in its surroundings.

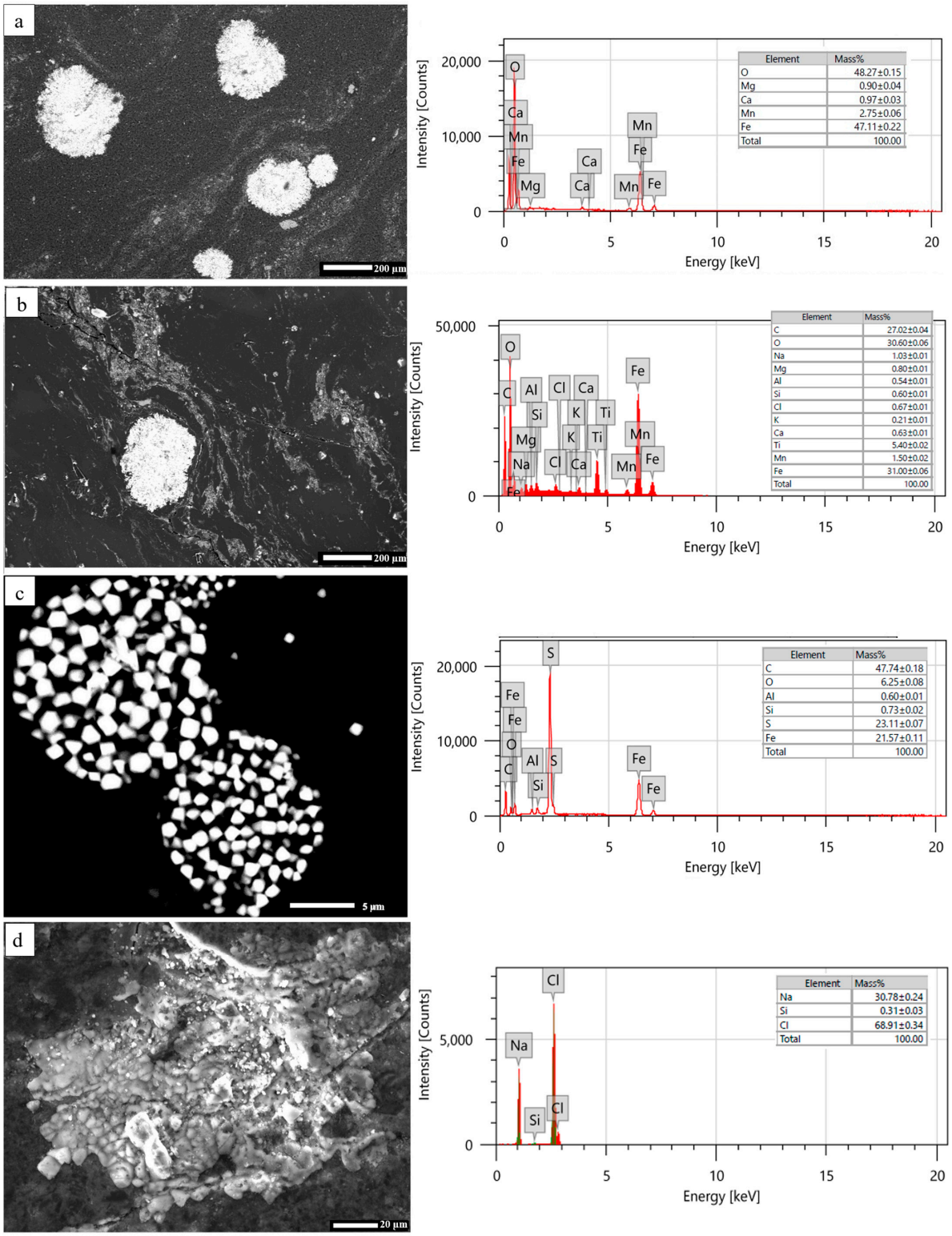


Figure 9. Selected SEM microphotographs (backscattered images, left side) of crystalline phases and EDS spectra (right side) of the studied coal samples of B1/0 (**a**) and S1 (**b**) for siderite; B1/1 for pyrite framboids (**c**), and B1/4 for halite (**d**).

Clay minerals, primarily kaolinite, are commonly found as infilling material in the pores of coal samples, making kaolinite the second most abundant mineral after quartz.

Several authors, including [60], have noted the widespread presence of kaolinite in coals. They suggest that kaolinite likely originates from the weathering of detrital materials and is commonly observed in the pores and cell cavities of coal samples. Kaolinite tends to develop readily in environments influenced by freshwater and acidic conditions. Renton [61] demonstrated that coals formed in freshwater depositional settings often contain abundant kaolinite. Renton [61] noted that kaolinite remains stable as a clay mineral in acidic freshwater environments.

Smectite clay mineral, primarily forms through the weathering alteration of volcanic ash rich in silica and aluminum, while illite forms through the chemical weathering of feldspar and the diagenetic alteration of smectite clays in the presence of potassium. Smectite suggests a significant volcanic influence due to its formation from altered volcanic material, while illite indicates a more mature sedimentary environment [62].

Euhedral pyrite is the predominant sulfide mineral across all coals, with its concentration varying among samples. It is more abundant than the framboidal pyrite and characterized by well-defined crystals in coals from both mine samples. The presence of euhedral pyrite as well-defined crystals suggests epigenetic processes, indicating depositional environments or post-depositional conditions favorable for crystalline growth [63,64]. The presence of euhedral pyrite and pyrite framboids, alongside very-low sulfur content, indicates complex depositional and diagenetic processes [50,65]. These features suggest varied environmental conditions during coal formation, possibly influenced by microbial activity and rapid mineral growth [50]. Sulfate minerals, such as barite, were very rare in the samples, as sulfate sulfur had a low value (average 0.1%, dry basis). Low sulfate sulfur values suggest that such minerals are rare or present in very small quantities [66]. Barite is found in association with smectite in coal samples. These associations occur because similar diagenetic conditions favor the formation of both barite and clay minerals [67,68].

Chalcopyrite is often coexisting with kaolinite crystal grains in all samples of both mines. The occurrence of chalcopyrite within kaolinite suggests during or after coal deposition, with kaolinite acting as a host mineral for chalcopyrite [58,69]. Other minerals coexisting with kaolinite crystals in coal samples include rare-earth element phosphate minerals. As [58] suggested, the co-occurrence of apatite with kaolinite crystals suggests that thermal fluids may have influenced their precipitation during or after coal formation. Additionally, the presence of detrital kaolinite, derived from weathering processes, provides a suitable host for the deposition of these phosphate minerals.

Other accessory minerals, such as rutile and anatase, are commonly observed as pore-filling minerals within the coal matrix and occasionally occur alongside kaolinite in the studied samples. This association suggests that the deposition of rutile and anatase likely occurred during or shortly after the formation of coal seams.

The abundance of detrital minerals in the coal samples suggests their likely deposition in terrestrial settings. Additionally, the very low total sulfur content (0.68%, whole-coal basis) observed in all coal samples suggests a non-marine origin, indicating deposition in lacustrine and swamp environments [69]. As previous studies [16,18] have confirmed, the KFC were deposited in fluvial and deltaic-lacustrine environments.

5.2. Sediment Source Region

The ratio of Al_2O_3/TiO_2 serves as a potential indicator for determining the source region of coal deposits [68,70]. This ratio is relatively stable during surface weathering and alteration processes [71,72]. In igneous rocks, Al is primarily found in feldspars, while Ti is associated with mafic minerals [73], making the Al_2O_3/TiO_2 ratio crucial for assessing the parent rock composition. Typically, a ratio of 3–8 suggests a mafic rock composition, while ratios of 8–21 and 21–70 indicate intermediate and felsic rocks, respectively [74].

Table 4 shows that the Al_2O_3/TiO_2 ratios observed in the coal samples range from 3.8 to 10.8, implying a sediment source in the studied coal samples derived from mafic and intermediate rocks.

5.3. Correlation of Ash Yields with Elements

The elemental composition of coal is influenced by the conditions during its formation and may change during the coalification process [75–77]. To determine the correlation of ash yields with elements in the studied samples from both mines, Pearson's correlation coefficients were utilized. The Pearson correlation coefficient matrix data indicates a clear division of elements, based on their correlation coefficients with ash yields. The positive correlation coefficients between the major elements and the ash yields were determined, e.g., TiO_2 and K_2O (with rash = 0.5–0.68) in the coals positively correlate with ash yields, indicating that these elements are predominantly associated with clay and iron dioxide minerals in all coal samples. Other major and trace elements (Al_2O_3, Na_2O, P_2O_5) and trace elements (Cd, La, Gd, B, Sm, Mn, Co, Pr, As and Nd) show very week and moderate positive correlations ranging from rash = 0.02–0.48. The remaining major elements (SiO_2, CaO, Fe_2O_3, and MgO) and trace elements (Ba, Cr, Yb, Pb, Cu, Eu, Li, Dy, Zn, Sr, V, Lu), moreover, and all sulfur forms (St, So, Ss and Sp) show a negative correlation with ash yield, ranging from rash = −0.1–−0.4.

Figure 10 shows, all forms of sulfur (between r =−0.01–−0.4), Fe2O3 (r= −0.13) and siderite (r = −0.79) exhibit a negative correlation with ash yield in the coals, additionally, as evidenced by a very low amount of sulfur content and the presence of siderite minerals as well. Siderite demonstrates a significantly positive correlation (r = 0.69) with Fe_2O_3. Fe_2O_3 exhibits a strong positive correlation (r = 0.81) with total sulfur (St) and a notable correlation (r = 0.70) with pyritic sulfur (Sp). Conversely, sulfate sulfur (Ss) shows a weak positive correlation (r = 0.26) with Fe_2O_3, while organic sulfur (So) displays a negligible correlation. Based on the correlation data, it is evident that Fe_2O_3 is predominantly associated with siderite and pyrite minerals.

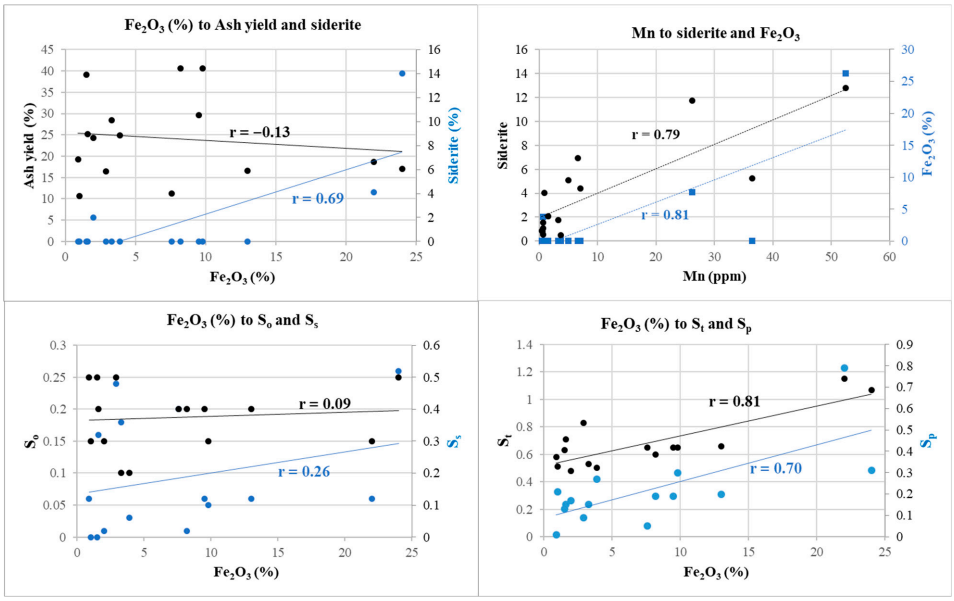


Figure 10. Relation of Fe2O3 to ash yield, siderite and Mn; and Fe_2O_3 to total sulfur (St), pyritic sulfur (Sp), organic sulfur (So), and sulfate sulfur (Ss).

Mn concentrations can vary based on the proximity to Mn-rich source rocks, as well as the geochemical conditions during coal accumulation [78]. Manganese in coal can be

associated with siderite, a mineral that often contains iron (Fe) and manganese. Siderite can act as a host for Mn in coal, where the presence of Mn may be linked to the depositional environment and geochemical conditions during coal formation. The association between Mn and siderite suggests that Mn may precipitate or co-occur with siderite minerals during peat accumulation and subsequent coalification processes. This confirms that Mn correlates positively (r = 0.79) with siderite and Fe_2O_3 (r = 0.81) in the samples from both mines (Figure 10), indicating a close association between Mn and siderite.

Figure 11 shows, the association of ash yield with major elements K_2O and TiO_2 shows positive correlations (r = 0.68 and r = 0.50, respectively), indicating the presence of titanium dioxide minerals (as determined by SEM-EDS) and clay minerals, predominantly illite, which shows a strong positive correlation (r = 0.72) with ash yield. In contrast, other clay minerals such as kaolinite and smectite exhibit negative correlations with ash yield (r = −0.21 and r = −0.4, respectively). The negative correlation between ash yield and clay minerals, as outlined by [71], reflects the well-established inverse relationship where higher clay mineral content. Different type and small size of clay minerals can influence their contribution to coal ash formation and subsequently affect ash yield measurements [79]. Quartz demonstrates a weak positive correlation with ash yield (r = 0.13), whereas it shows a negative correlation with SiO_2 (r = −0.34). The negative correlation observed between SiO_2 content and ash yield in coal samples, as suggested by [80], indicates that higher SiO_2 content in coal is not associated with an increased presence of authigenic minerals such as pyrite, halite, and sulfate minerals. These minerals typically form under distinct geochemical conditions within coal seams, which are independent of the SiO_2 content of the coal. This can be scientifically explained by considering the mineralogical composition and behavior of silicon dioxide during coal formation and combustion processes. As [78,81,82] mentioned that the weak correlation between ash yield and quartz/SiO_2 can be attributed to variations in mineralogical composition and distribution within coal samples. A study by [79] highlighted significant variability in quartz content in coals indicating that quartz concentration is not solely dependent on total ash yield but also on the inherent mineralogy of the coal. This variability underscores the complex relationship between coal composition and ash mineral content.

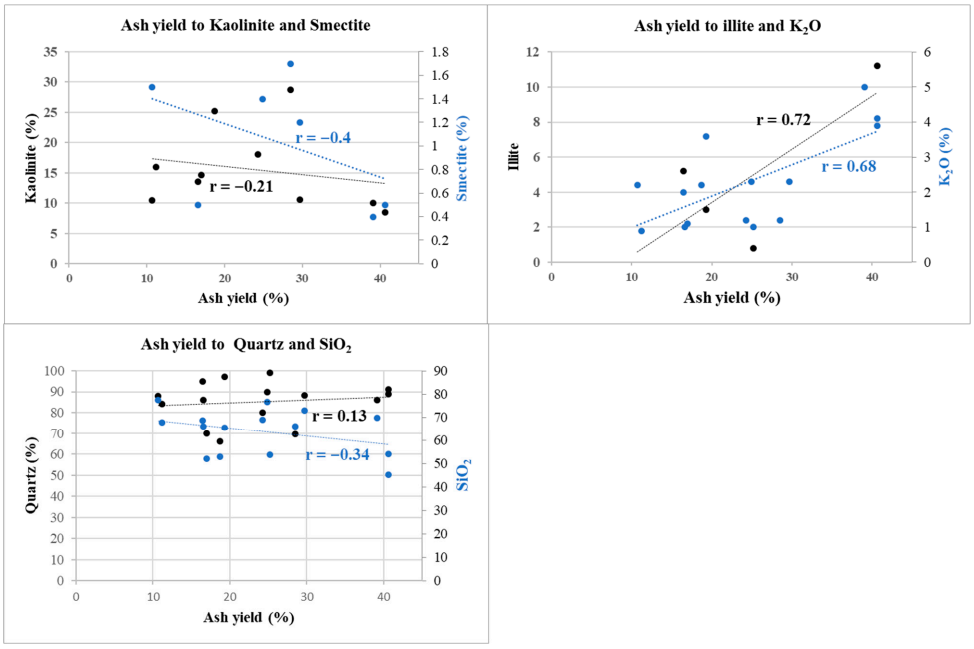


Figure 11. Relation of ash yield to quartz and clay minerals: kaolinite and smectite; illite and K_2O; and quartz and SiO_2.

5.4. Modes of Occurrence of Enriched Valuable Sm and Lu and Elements in Coals

Understanding the sources and modes of occurrence of the elemental enrichment and distribution in coals is crucial for assessing its economic potential. Rare earth elements (REEs) including Samarium (Sm), and Lutetium (Lu) are found in trace amounts in coal samples of both mines.

The enrichment of Sm and Lu in coal are generally low, typically in ppm or even ppb range [78], and their distribution within coal seams is often heterogeneous, influenced by the depositional environment and geochemical conditions during and after peat formation [83–86]. Both Sm and Lu can be associated with the organic matrix of coal, where complexation with organic molecules, such as humic substances, influences their distribution and concentration [83,87–89]. Lu shows a positive correlation of 0.5 with the organic component, whereas Sm exhibits a negative correlation (r = −0.4) (Figure 12). Both Lu and Sm display negative correlations with P_2O_3 (r = −0.02 and r = −0.19) in the samples.

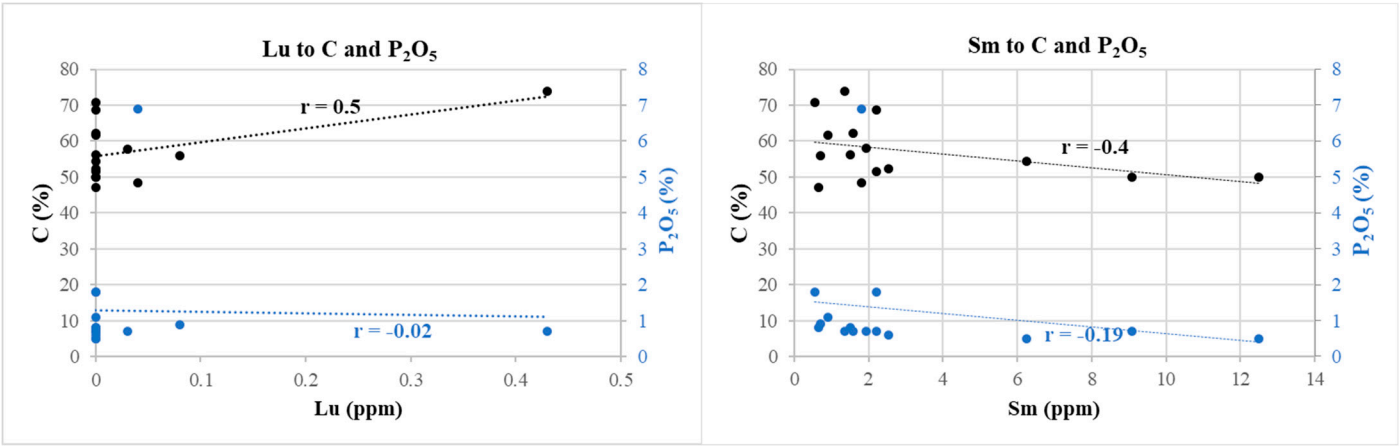


Figure 12. Relation of Lu and Sm to organic carbon (C) and P_2O_5.

Coal formed in specific depositional environments, such as lacustrine settings, often shows elevated levels of REEs, including Sm and Lu [78,90–92]. The type of source rock from which the coal originates significantly affects the concentrations of Sm and Lu; intermediate and mafic igneous rocks are typically rich in REEs, and weathering and erosion of these rocks release REEs into the environment, which are then transported and incorporated into coal deposits [88,93–95].

5.5. Comparison with Previous Studies on Kazakhstani Ash and Slag Materials

The chemical and mineralogical composition of our samples, particularly the elevated SiO_2 and Al_2O_3 contents and quartz–kaolinite dominance, suggests potential for valorization pathways similar to those reported by authors [96] who examined ash and slag residues from Kazakhstan's fuel-energy sector. Authors [96] highlighted that materials with high silica–alumina ratios and moderate Fe_2O_3 contents can serve as precursors for geopolymers, ceramic materials, zeolite synthesis, and construction products. The SiO_2/Al_2O_3 ratios observed in our samples are comparable to their reported values, indicating that, despite the relatively high crystallinity of quartz, the kaolinite-rich fractions could be reactive under appropriate activation conditions (e.g., dehydroxylation to metakaolin).

Furthermore, recent work by authors [97] examined ash and slag waste from Kazakhstani deposits specifically in the context of developing construction products. Their study emphasizes technological considerations such as particle size distribution, phase composition, and oxide ratios, which influence the suitability of ash and slag for concrete additives, lightweight aggregates, and other building materials. The compositional and

mineralogical trends observed in our KCF ash samples—particularly elevated SiO_2 and Al_2O_3 contents and quartz–kaolinite dominance—align with the parameters identified by [97] as favorable for construction applications. This comparison reinforces the industrial relevance of our findings and supports further research into processing and application optimization of these coal-derived materials.

These parallels suggest that the mineralogical and chemical trends identified in our study may support similar technological applications, providing a rationale for further research into the practical utilization of these coal-derived materials.

6. Conclusions

In this study, mineralogical and geochemical analyses were conducted on Carboniferous bituminous coals from the Karagandy Coal Formation (KCF), including samples from the Bogatyr and Saradyr mines in North-Eastern Kazakhstan, using ash yield and organic elemental analyses, FTIR, XRD, SEM-EDS, and ED-XRF. The key findings are as follows:

(1) The coal is predominantly composed of quartz and clay minerals (kaolinite, smectite, and illite), with minor pyrite. Accessory minerals include phosphate minerals (apatite), chalcopyrite, siderite, halite, rutile, and ilmenite. The occurrence of both detrital and authigenic minerals suggests a terrestrial depositional environment under freshwater-influenced conditions.

(2) The mode of occurrence and morphology of detrital and authigenic minerals indicate accumulation with weathering during or shortly after peat deposition in lacustrine and wetland environments.

(3) Twenty-four trace elements were identified, with Mn (23.8 ppm) and Sm (6.3 ppm) being the most abundant, followed by Ba, Zn, Sr, V, Pb, B, As, Ce, Li, Nd, and Cu. Rare earth elements and Y ranged from 7.5 to 39.2 ppm (average 25.3 ppm).

(4) Of industrial interest, Sm is slightly enriched (CC = 2.8), Lu shows normal concentration (CC < 1), and the remaining trace elements are depleted (CC < 0.5) in samples from both mines.

(5) Al_2O_3/TiO_2 ratios (3.8–10.8) suggest mineral and elemental enrichments originated from intermediate and mafic sources. Combined with detrital composition and high ash content, this indicates substantial accommodation space during or immediately after peat accumulation. The elevated SiO_2 and Al_2O_3 contents and quartz–kaolinite mineralogy of KCF ash highlight promising potential for industrial applications, including geopolymers, ceramics, zeolites, and construction materials, supporting environmentally and economically valuable utilization of these coal resources.

Future studies could include roof and floor-rock petrography, organic petrography, and palynological analyses to further constrain paleodepositional conditions and paleoclimate, providing additional insights for both scientific and industrial applications.

Author Contributions: Conceptualization, M.J. and A.H.M.; Methodology, M.J., A.H.M. and M.A.O.; Software, M.J., Y.N. and M.A.O.; Validation, M.J., A.H.M., Y.N., M.A.O. and Z.T.U.; Formal analysis, M.J., Y.N., M.A.O. and Z.T.U.; Investigation, M.J.; Resources, M.J., A.H.M. and Y.N.; Data curation, M.J.; Writing—original draft, M.J.; Writing—review and editing, M.J.; Visualization, M.J.; Supervision, M.J.; Project administration, G.Z.Z.; Funding acquisition, G.Z.Z.; Validation, M.A.M.; Validation, K.T. All authors have read and agreed to the published version of the manuscript.

Funding: This research is funded by the Committee of Science of the Ministry of Science and Higher Education of the Republic of Kazakhstan (Grant No. BR27199165). BR27199165 Scientific substantiation of the expansion and replenishment of mineral resources of priority and critical minerals as the basis for the innovative development of Kazakhstan.

Data Availability Statement: The data presented in this study are available on request from the corresponding authors. All data are new data datasets are stored and can be shared for academic and research purposes. No publicly archived datasets were generated during this study.

Conflicts of Interest: The authors declare no conflicts of interest.

References

1. Finkelman, R.B. Coal rank, a measure of coalification. In *Coal: Typology, Chemistry, Physics, Constitution*; Elsevier: Amsterdam, The Netherlands, 1994; pp. 163–179.
2. Finkelman, R.B. Modes of occurrence of potentially hazardous elements in coal: Levels of confidence. *Fuel Process. Technol.* **2004**, *85*, 1215–1247. [CrossRef]
3. Finkelman, R.B. Medical geology: A global perspective. *Environ. Geochem. Health* **2004**, *26*, 193–199.
4. Dai, S.; Jiang, Y.; Ward, C.R.; Hower, J.C.; Yan, X.; Zhu, X.; Li, T. Major and trace elements in Chinese coals: A national database and their geochemical implications. *Int. J. Coal Geol.* **2020**, *218*, 103331.
5. Liu, G.; Lai, Y.; Zhao, L.; Yan, X. Geochemistry of rare earth elements in Chinese coals. *Fuel* **2005**, *84*, 426–430.
6. Liu, Z.; Jiang, Y.; Wang, H.; Wang, X.; Zhang, Y.; Liu, G. The chemical characteristics of rare earth elements in Chinese coals. *Int. J. Coal Geol.* **2018**, *187*, 22–33.
7. Ketris, M.P.; Yudovich, Y.E. Estimations of Clarkes for carbonaceous biolithes: World averages for trace element contents in black shales and coals. *Int. J. Coal Geol.* **2009**, *78*, 135–148. [CrossRef]
8. Karayiğit, A.I.; Bircan, C.; Mastalerz, M. Coal characteristics, elemental composition and modes of occurrence of some elements in the İsaalan coal (Balıkesir, NW Turkey). *Int. J. Coal Geol.* **2017**, *172*, 43–59. [CrossRef]
9. Hower, J.C.; Berti, D.; Hochella, M.F. Submicron-scale mineralogy of lithotypes and the implications for trace element associations: Blue Gem coal, Knox County, Kentucky. *Int. J. Coal Geol.* **2018**, *192*, 73–82. [CrossRef]
10. Ward, C.R. The occurrence and geochemistry of siderite in some Australian coals. *Int. J. Coal Geol.* **2002**, *50*, 421–438.
11. Ward, C.R. Petrology and geochemistry of coal. In *Coal and Peat Fires: A Global Perspective 3*; Schobert, H.D., Hwang, S.S., Matheus, J.M., Eds.; Elsevier: Amsterdam, The Netherlands, 2016; pp. 81–126.
12. Harvey, H.R.; Ruch, R.R. Classification of inorganic constituents of coals: An organochemical approach. *Org. Geochem.* **1986**, *10*, 61–76.
13. Seredin, V.V.; Finkelman, R.B. Metalliferous coals: A review of the main genetic and geochemical types. *International J. Coal Geol.* **2008**, *76*, 253–289. [CrossRef]
14. Seredin, V.V.; Dai, S. Coal deposits as potential alternative sources for lanthanides and yttrium. *Int. J. Coal Geol.* **2012**, *94*, 67–93. [CrossRef]
15. Dai, S.; Finkelman, R.B. Coal as a promising source of critical elements: Progress and future prospects. *Int. J. Coal Geol.* **2017**, *182*, 155–164. [CrossRef]
16. Ammosov, I.I.; Burcev, D.N.; Gorsky, I.I.; Ivanov, G.A.; Kotlukov, V.A.; Kuznecov, I.A.; Lugovoy, G.I.; Mironov, K.V.; Molchanov, I.I.; Nekipelov, B.E.; et al. *Geology of Coal and Black Deposits*; Nedra: Moscow, Russia, 1973; pp. 13–718. (In Russian)
17. Ammosov, I.I.; Burcev, D.N.; Gorsky, I.I.; Ivanov, G.A.; Kotlukov, V.A.; Kuznecov, I.A.; Lugovoy, G.I.; Mironov, K.V.; Molchanov, I.I.; Nekipelov, B.E.; et al. *Geology of Coal and Black Deposits*; Nedra: Moscow, Russia, 1973; pp. 2–219. (In Russian)
18. Azizov, T.M.; Vlasov, Y.I. *Coal and Oil Shale Basins and Deposits of Kazakhstan*; AB Bekturov Institute of Chemical Sciences JS: Almaty, Kazakhstan, 2013; pp. 6–106.
19. EIA Report 2017. Available online: https://www.ieee.es/en/Galerias/fichero/OtrasPublicaciones/Internacional/2017/EIA_Country_Aanlysis_Kazakhstan_10may2017.pdf (accessed on 16 March 2024).
20. Amangeldikyzy, A.; Kopobayeva, A.N.; Blyalova, G.G.; Askarova, N.S. Geochemical speciation of coals in the Karaganda coal Basin. *Min. J. Kazakhstan* **2023**, *7*, 15–20.
21. Kopobayeva, A.; Baidauletova, I.; Amangeldikyzy, A.; Askarova, N. Trace elements distribution in the k_7 seam of the Karaganda Coal Basin, Kazakhstan. *Geosciences* **2024**, *14*, 143. [CrossRef]
22. Kopobayeva, A.; Amangeldikyzy, A.; Blyalova, G.; Askarova, N. Mineralogical and geochemical features of coals and clay layers of the Karaganda Coal Basin. *Minerals* **2024**, *14*, 349. [CrossRef]
23. Junussov, M.; Tarikhov, F.; Abildakhanov, A.; Zhanaidar, D.; Mekenbek, G.; Assambayeva, A. Mineralogical and elemental analysis of Kazakh coals from three mines: Preliminary insights from mode of occurrence to environmental impacts. *Open Geosci.* **2024**, *16*, 20220721. [CrossRef]
24. Junussov, M.; Mustapayeva, S. Preliminary XRF analysis of coal ash from Jurassic and Carboniferous coals at five Kazakh mines: Industrial and environmental comparisons. *Appl. Sci.* **2024**, *14*, 10586. [CrossRef]

25. Safaei-Farouji, M.; Misch, D.; Sachsenhofer, R.F.; Weitz, J.; Kojic, I.; Stojanović, K.; Tursyngaliyev, S.; Junussov, M.; Fustic, M. Organic petrography and geochemistry of the Lower-Carboniferous coals from the Ekibastuz Basin, Kazakhstan. *Int. J. Coal Geol.* **2025**, *306*, 104813. [CrossRef]
26. David, B.R.; Anne, R.; Judith, T.P.; Ann, L.L.; Christopher, R.S.; Alfred, M.Z. Carboniferous paleogeographic, phytogeographic and paleoclimatic reconstructions. *Int. J. Coal Geol.* **1985**, *5*, 7–42. [CrossRef]
27. *ISO 7404-2*; Methods for the Petrographic Analysis of Bituminous Coal and Anthracite—Part 2: Methods for Preparing Coal Samples. International Organization for Standardization: Geneva, Switzerland, 2009; 12p.
28. *ASTM STM D2013/D2013M-12*; Standard Practice for Preparing Coal Samples for Analysis. ASTM International: West Conshohocken, PA, USA, 2012.
29. Han, Q.; Liu, J.; Shang, N.; Zhao, S.; Jia, R. Optimization of Operating Parameters for Coal Low-Temperature Ashing: A Suitable and Efficient Treatment Method for Mineral Analysis in Coal. *Minerals* **2022**, *12*, 1119. [CrossRef]
30. Qi, D.; Wu, S.; Li, S.; Zhao, G.; Xing, J.; Kang, S.; Wang, Q.; Gao, W. Enrichment Characteristics, Occurrence and Origin of Valuable Trace Elements in Lignite from Linchang Coal Mine, Guangxi, China. *J. Geosci. Environ. Prot.* **2021**, *9*, 12. [CrossRef]
31. *ASTM D3173-11*; Standard Test Method for Moisture in the Analysis Sample of Coal and Coke. ASTM International: West Conshohocken, PA, USA, 2011.
32. *ASTM D3174-12*; Standard Test Method for Ash in the Analysis Sample of Coal and Coke from Coal. American Society for Testing and Materials: West Conshohocken, PA, USA, 2013; pp. 498–503.
33. *ASTM D3175–11*; Standard Test Method for Volatile Matter in the Analysis Sample of Coal and Coke. ASTM International: West Conshohocken, PA, USA, 2011.
34. *ASTM D5373-16*; Standard Test Methods for Determination of Carbon, Hydrogen and Nitrogen in Analysis Samples of Coal and Carbon in Analysis Samples of Coal and Coke. ASTM International: West Conshohocken, PA, USA, 2016.
35. Mesroghli, S.; Jorjani, E.; Chelgani, S.C. Estimation of Gross Calorific Value Based on Coal Analysis Using Regression and Artificial Neural Networks. *Int. J. Coal Geol.* **2009**, *79*, 49–54. [CrossRef]
36. Munshi, T.A.; Jahan, L.N.; Howladar, M.F.; Hashan, M. Data-driven computational approaches to estimate gross calorific value of coal using proximate and ultimate analyses. *Int. J. Coal Prep. Util.* **2024**, *44*, 1653–1678. [CrossRef]
37. *ASTM D2492-02*; Standard Test Method for Forms of Sulfur in Coal. ASTM International: West Conshohocken, PA, USA, 2002.
38. *ASTM D3177–02*; Standard Test Methods for Total Sulfur in the Analysis Sample of Coal and Coke. ASTM International: West Conshohocken, PA, USA, 2002; Reapproved 2007.
39. Yang, Y.; Wei, X.; Wang, H.; Ma, D. Characterization of coal ash from thermal power plants in China and its environmental impact assessment. *Fuel* **2015**, *143*, 39–45.
40. Rietveld, H.M. A profile refinement method for nuclear and magnetic structures. *J. Appl. Crystallogr.* **1969**, *2*, 65–71. [CrossRef]
41. Taylor, J.C. Computer programs for standardless quantitative analysis of minerals using the full powder diffraction profile. *Powder Diffr.* **1991**, *6*, 2–9. [CrossRef]
42. Tian, X.; Zhao, L. Determination of concentrations of Sr and Ba in coal and coal combustion by-products: A comparison between results by ICP-MS and XRF techniques. *Talanta* **2024**, *266*, 124919. [CrossRef] [PubMed]
43. Matsunami, H.; Matsuda, K.; Yamasaki, S.I.; Kimura, K.; Ogawa, Y.; Miura, Y.; Tsuchiya, N. Rapid simultaneous multi-element determination of soils and environmental samples with polarizing energy dispersive X-ray fluorescence (EDXRF) spectrometry using pressed powder pellets. *Soil Sci. Plant Nutr.* **2010**, *56*, 530–540. [CrossRef]
44. Wang, J.; Nakazato, T.; Sakanishi, K.; Yamada, O.; Tao, H.; Saito, I. Microwave digestion with HNO_3/H_2O_2 mixture at high temperatures for determination of trace elements in coal by ICP-OES and ICP-MS. *Anal. Chim. Acta* **2004**, *514*, 115–124. [CrossRef]
45. Chen, C.; Zou, M.; Mastalerz, M.; Hu, S.; Gasaway, C.; Tao, X. Applications of micro-fourier transform infrared spectroscopy (FTIR) in the geological sciences—A Review. *Int. J. Mol. Sci.* **2015**, *16*, 30223–30250. [CrossRef]
46. Davis, B.A.; Rodrigues, S.; Esterle, J.S.; Rintoul, L.; Duxbury, A.J.; Golding, S.D. In situ techniques for classifying apatite in coal. *Int. J. Coal Geol.* **2020**, *230*, 103572. [CrossRef]
47. Srivastava, M.K.; Kishor, K.; Nath, M.; Singh, A.K. Inorganic geochemical attributes of Jaintia Hills coals, India: Implications for paleo-depositional conditions. *Kuwait J. Sci.* **2024**, *51*, 100227. [CrossRef]
48. Jenkins, R.G.; Walker, P.L., Jr. Analysis of Mineral Matter in Coal. In *Analytical Methods for Coal and Coal Products*; Chapter 26; Academic Press: Cambridge, MA, USA, 1978; Volume II, pp. 265–292.
49. Dai, S.; Li, T.; Jiang, Y.; Ward, C.R.; Hower, J.C.; Sun, J.; Liu, J.; Song, H.; Wei, J.; Li, Q.; et al. Mineralogical and geochemical compositions of the Pennsylvanian coal in the Hailiushu Mine, Daqingshan Coalfield, Inner Mongolia, China: Implications of sediment-source region and acid hydrothermal solutions. *Int. J. Coal Geol.* **2015**, *137*, 92–110. [CrossRef]
50. Ingham, J.K.; Davies, G.R.; Taylor, P.N. 3D microtexture analysis of pyrite framboids in coal: Understanding modes of formation. *Int. J. Coal Geol.* **2013**, *115*, 19–34.
51. Goodarzi, F.; Swaine, D.J. Environmental Aspects of Trace Elements in Coal. *Environ. Geochem. Health* **1994**, *16*, 67–82.
52. Hower, J.C.; Eble, C.F.; Cobb, J.C. Siderite in coal and associated strata. *Int. J. Coal Geol.* **1991**, *18*, 3–20.

53. Dai, S.; Fang, C.; Zhou, J.; Liu, H.; Wang, X.; Zhan, X. Sulfur forms in coals of China. *Int. J. Coal Geol.* **2002**, *50*, 135–152.
54. Hower, J.C.; Eble, C.F.; O'Keefe, J.M.K.; Dai, S.; Wang, P. Petrology, Palynology, and Geochemistry of Gray Hawk Coal (Early Pennsylvanian, Langsettian) in Eastern Kentucky, USA. *Minerals* **2015**, *5*, 592–622. [CrossRef]
55. Ward, C.R. Pyrite framboids in coal: An overview. *Int. J. Coal Geol.* **1984**, *3*, 279–307.
56. Scott, A.C. Charcoal recognition, taphonomy and uses in palaeoenvironmental analysis. *Palaeogeogr. Palaeoclimatol. Palaeoecol.* **2010**, *291*, 11–39. [CrossRef]
57. Hower, J.C. Halite in Coal: Significance and Implications. *Int. J. Coal Geol.* **1999**, *40*, 89–107.
58. Ward, C.R.; French, D. Clay minerals in coal-fired sediments and sedimentary rocks: A review. *Int. J. Coal Geol.* **2006**, *67*, 2–18. [CrossRef]
59. Smith, K.L.; Smoot, L.D. Characteristics of commonly-used US coals—Towards a set of standard re-search coals. *Prog. Energy Combust. Sci.* **1990**, *16*, 1–53. [CrossRef]
60. Ribeiro, L.; Sharygin, I.; Karpinsky, G.; Krivovichev, S.; Platonov, Y.; Zhukhlistova, I.; Seryotkin, S. Comparative study of framing framboidal and non-framboidal pyrite in Permian coal samples from the Kuznetsk Basin, Russia. *Minerals* **2019**, *9*, 303.
61. Renton, J.J. 7—Mineral Matter in Coal. In *Coal Structure*; Meyers, R.A., Ed.; Academic Press: Cambridge, MA, USA, 1982; pp. 283–326.
62. Spears, D.A.; Zheng, Y. Geochemistry and origin of elements in some UK coals. *Int. J. Coal Geol.* **1999**, *38*, 161–179. [CrossRef]
63. Hower, J.C.; Blake, D.J.; Howell, D.K.; Lawton, T.E.; Martin, H.P. Framboidal pyrite formation in coal: An SEM investigation of microstructure. *Int. J. Coal Geol.* **2015**, *142*, 13–21.
64. Hower, J.C.; Rimmer, S.M.; Eble, C.F.; Freeman, P.A.; Stucker, J.D. The nature of pyrite in some Appalachian coals. *Int. J. Coal Geol.* **2015**, *147–148*, 104–115.
65. Filho, J.G.S.; Hu, Y.; Lee, C.T.A.; Youbi, N. Low-sulfur coals from the Late Permian Gangra coalfield, the Yarlung–Tsangpo suture zone, southern Tibet: Origin and implications for tectonic setting. *Int. J. Coal Geol.* **2013**, *109–110*, 85–98.
66. Finkelman, R.B. Potential Health Impacts of Burning Coal Beds and Waste Banks. *Int. J. Coal Geol.* **2004**, *59*, 19–24. [CrossRef]
67. Goodarzi, F. Morphology and chemistry of fine particles emitted from a Canadian coal-fired power plant. *Fuel* **2006**, *85*, 273–280. [CrossRef]
68. Hower, J.C.; Ruppert, L.F. Splint coals of the Central Appalachians: Petrographic and geochemical facies of the Peach Orchard No. 3 split coal bed, southern Magoffin County, Kentucky. *Int. J. Coal Geol.* **2011**, *85*, 268–275. [CrossRef]
69. Moore, F.; Esmaeili, A. Mineralogy and geochemistry of the coals from the Karmozd and Kiasar coal mines, Mazandaran province, Iran. *Int. J. Coal Geol.* **2012**, *96–97*, 9–21. [CrossRef]
70. Belkin, H.E.; Tewalt, S.J. Geochemistry of Selected Coal Samples from Sumatra, Kalimantan, Sulawesi, and Papua, Indonesia. US Geological Survey. 2007; 34p. Available online: https://pubs.usgs.gov/publication/ofr20071202 (accessed on 22 December 2025).
71. Grim, R.E. *Clay Mineralogy*; McGraw-Hill Book Company: New York, NY, USA, 1962.
72. Guo, W.; Dai, S.; Nechaev, V.P.; Nechaeva, E.V.; Wei, G.; Finkelman, R.B.; Spiro, B.F. Geochemistry of Palaeogene coals from the Fuqiang Mine, Hunchun Coalfield, northeastern China: Composition, provenance, and relation to the adjacent polymetallic deposits. *J. Geochem. Explor.* **2019**, *196*, 192–207. [CrossRef]
73. Wang, J.; Shao, L.; Yan, A.; Wang, X. The coal-forming environment during mass extinction in the latest permian: Evidence from geochemistry of rare Earth elements. *Front. Earth Sci.* **2023**, *10*, 1057831. [CrossRef]
74. Hayashi, K.I.; Fujisawa, H.; Holland, H.D.; Ohmoto, H. Geochemistry of ~1.9 Ga sedimentary rocks from northeastern Labrador, Canada. *Geochim. Cosmochim. Acta* **1997**, *61*, 4115–4137. [CrossRef]
75. Saxby, J.D. Minerals in coal. In *Organic Matter and Mineralisation: Thermal Alteration, Hydrocarbon Generation and Role in Metallogenesis*; Glikson, M., Mastalerz, M., Eds.; Springer Netherlands: Berlin/Heidelberg, Germany, 2000; pp. 314–328.
76. Junussov, M. Characteristics, distribution and morphogenesis of gold-bearing sulfde minerals in the gold black shale deposit of Bakyrchik. In Proceedings of the 18th International Multidisciplinary Scientifc Geoconference Surveying Geology and Mining Ecology Management, SGEM, Albena, Bulgaria, 2–8 July 2018; Volume 18, pp. 643–650. [CrossRef]
77. Junussov, M.; Mohammad, A.; Longinos, S. Geochemical analysis of organic matter associated with gold in ore deposits: A study of Kazakhstan and Hungary. *Acta Geochim.* **2025**, *44*, 23–35. [CrossRef]
78. Dai, S.; Seredin, V.V.; Ward, C.R.; Hower, J.C.; Xing, Y.; Zhang, W.; Song, W.; Wang, P. Enrichment of U–Se–Mo–Re–V in coals preserved within marine carbonate successions: Geochemical and mineralogical data from the Late Permian Guiding Coalfield, Guizhou, China. *Miner. Depos.* **2015**, *50*, 159–186. [CrossRef]
79. Ward, C.R.; French, D.; Kuehn, S.C.; Mark, C. Variability in ash chemistry and mineralogy in Australian coals: Implications for ash utilisation. *Int. J. Coal Geol.* **2018**, *186*, 130–142. [CrossRef]
80. Vassilev, S.V.; Vassileva, C.G.; Baxter, D.; Andersen, L.K. Relationships between chemical and mineral composition of coal and their potential applications as genetic indicators. *Geol. Balanica* **2010**, *39*, 21–41. [CrossRef]
81. Speight, J.G. *The Chemistry and Technology of Coal*; CRC Press: Boca Raton, FL, USA, 2013.

82. Junussov, M.; Abirov, R.; Mekenbek, G.; Assambayeva, A.; Mukhamediyarova, N. New insights into pyrite in the Western Mecsek uranium ore deposit: Its morphology, invisible gold and trace element composition. *Bull. Miner. Res. Explor.* **2025**, *177*, 1–2. [CrossRef]
83. Vassilev, S.V.; Vassileva, C.G.; Karayiğit, A.I. Contents, modes of occurrence, and origin of chlorine and bromine in coal. *Fuel* **2010**, *89*, 811–824. [CrossRef]
84. Zhao, C.; Zheng, Y.; Zhang, C.; Zhang, L. Rare earth elements in Chinese coals. *Fuel* **2007**, *86*, 584–591.
85. Junussov, M.; Ferenc, M.; Ferenc, K.; Tivadar, T.; Krisztián, F.; Gábor, M.; Ádám, P.; Mária, H.V. Preliminary analysis on roles of metal–organic compounds in the formation of invisible gold. *Acta Geochim.* **2021**, *40*, 1050–1072. [CrossRef]
86. Junussov, M.; Mádai, F.; Földessy, J.; Hámor-Vidó, M. The role of organic matter in gold occurrence: Insights from western mecsek uranium ore deposit. *Econ. Environ. Geol.* **2024**, *57*, 371–386. [CrossRef]
87. Junussov, M.; Kembayev, M.K.; Rais, S.E.; Amantayev, A.; Biyakyshev, Y.; Akbarov, E.; Mekenbek, G.; Kokkuzova, M.; Baisalova, A.; Pan, J. Process Evolution and Green Innovation in Rare Earth Element Research: A 50-Year Bibliometric Assessment (1975–2024). *Processes* **2026**, *14*, 41. [CrossRef]
88. Jordens, A.; Cheng, Y.P.; Waters, K.E. A review of the beneficiation of rare earth element bearing minerals. *Ore Geol. Rev.* **2013**, *41*, 97–114. [CrossRef]
89. Junussov, M.; Kembayev, M.; Mukhamediyarova, N.; Rustembekov, M.M.; Abirov, A. Trace element geochemistry of dispersed organic matter in Western Mecsek uranium ore deposit, Southern Hungary. *Acta Geochim.* **2025**, 1–21. [CrossRef]
90. Asif, M.; Junussov, M.; Longinos, S.; Hazlett, R.; Satibekova, S. CO_2 storage capacity of coal seams: A screening and geological review of carboniferous coal formations of Kazakhstan. *Int. J. Coal Sci. Technol.* **2025**, *12*, 18. [CrossRef]
91. Junussov, M.; Kembayev, M.K.; Mekenbek, G.; Mukhamediyarova, N.; Kokkuzova, M.; Assambayeva, A.; Abirov, R. Four decades of trends in invisible gold research: A web of science-based bibliometric analysis (1985–2024). *Earth Sci. Inform.* **2025**, *18*, 484. [CrossRef]
92. Arbuzov, S.I.; Volostnov, A.V.; Rikhvanov, L.P.; Mezhibor, A.M.; Ilenok, S.S. Geochemistry of radioactive elements (U, Th) in coal and peat of northern Asia (Siberia, Russian Far East, Kazakhstan, and Mongolia). *Int. J. Coal Geol.* **2011**, *86*, 318–328. [CrossRef]
93. Junussov, M.; Kembayev, K.M.; Kokkuzova, M.; Baisalova, A.; Umarbekova, T.Z.; Abirov, R.; Rais, E.S.; Amantayev, A. Exploring rare earth elements in Northern Kazakhstan: The potential of ion-adsorption clays and coals as unconventional sources. *Acta Geochim.* **2025**, *in press*. [CrossRef]
94. Longinos, S.N.; Serik, A.; Bayramov, E.; Junussov, M.; Begaliyev, D.; Hazlett, R. Laboratory Study of Liquid Nitrogen Cryo-Fracturing as an Environmentally Friendly Approach for Coalbed Methane (CBM) Reservoirs. *Energies* **2024**, *17*, 2359. [CrossRef]
95. Safaei-Farouji, M.; Misch, D.; Sachsenhofer, R.F.; Kostoglou, N.; Gaus, G.; Bauersachs, T.; Junussov, M.; Fustic, M. CO_2 utilization and sequestration potential in deep coal seams: A case study on carboniferous coals from the Karaganda basin, kazakhstan. *J. CO_2 Util.* **2025**, *101*, 103204. [CrossRef]
96. Nurmakova, S.; Sarsembin, U.; Dalbanbay, A.; Abilova, G.; Tusupova, B.; Kurbanova, L.; Zharkimbaeva, G.; Shanbayev, M. Innovative approaches to the processing of ash and slag materials from the fuel and energy sector in the context of sustainable development. *Eng. J. Satbayev Univ.* **2025**, *147*, 30–39. [CrossRef]
97. Nurpeisova, M.; Estemesov, Z.; Gabbasov, S.; Ashimova, A.; Bek, A. Studying the properties of ash and slag waste for use in the manufacture of construction products. *Min. Miner. Depos.* **2023**, *17*, 102–109. [CrossRef]

Disclaimer/Publisher's Note: The statements, opinions and data contained in all publications are solely those of the individual author(s) and contributor(s) and not of MDPI and/or the editor(s). MDPI and/or the editor(s) disclaim responsibility for any injury to people or property resulting from any ideas, methods, instructions or products referred to in the content.